Label-free Optical Single-Molecule Micro- and Nano-Sensors

Sivaraman Subramanian*[1], Hsin-Yu Wu*[1], Tom Constant*[1], Jolly Xavier*[1], Frank Vollmer[1]*

[1] Living Systems Institute, Department of Physics and Astronomy, University of Exeter, EX4 4QD, UK

*corresponding authors' email addresses: ss905@exetert.ac.uk, h.wu@exeter.ac.uk, t.j.constant@exeter.ac.uk, j.xavier@exeter.ac.uk, f.vollmer@exeter.ac.uk;

Introduction

Single-molecule techniques continue to transform imaging, biophysics and, more recently, optical sensing. Label-free optical sensor systems have emerged that exhibit extraordinary sensitivity for detecting physical, chemical, and biological entities at the micro/nanoscale. Particularly exciting is the detection and analysis of molecules on micro and nanoscale optical transducers that can be integrated and multiplexed on miniature sensing devices and that have many possible applications in health, environment, and security. It is also becoming increasingly clear that in order for us to better understand the functionality of complex bio-molecules, we need to investigate their dynamics.[1] X-ray crystallography and dramatic advances in electron microscopy[2] have led to the structural identification of a large number of biomolecules.[3] However, accessing the dynamic information has been more challenging owing to the wide timescales and range of motions involved.[1] Nonetheless, a variety of techniques such as small-angle X-ray scattering (SAXS),[4] nuclear magnetic resonance (NMR) spectroscopy,[5] and mass spectrometry[6] have provided critical information on biomolecular conformational dynamics in the past three decades. However, these techniques are mostly ensemble methods, which require a large number of molecules for measurement. Hence, these methods

suppress molecular heterogeneity, that is, they do not report fluctuations of a molecular property from the mean value.[7] In the optical domain, the most popular technique is fluorescence spectroscopy, which has the capability to detect single molecules, and report on molecular conformations via Forster Resonance Energy Transfer (FRET).[8, 9] The large range of fluorescent dyes, combined with optimized optics, efficient detectors and algorithms have made single-molecule fluorescence spectroscopy the method of choice for single molecule dynamic studies in the past decade.[9] However, this technique requires the labelling of the molecules of interest which can be a drawback in certain investigations. In some cases, it might not be possible to attach a label,[10] or the label might affect the kinetics[11] of the molecules under study.

Fortunately, a new class of label-free micro and nanosensors are starting to emerge that might allow us to do exactly that, observe dynamic processes at the single molecule level directly with light, with high temperal and spatial resolution without the use of flourescent labels. Hence, these sensors will be complementary to the existing well established techniques such as NMR, mass spectrometry and flourescence spectrosopy in the near future. Micro- and nanosensors by virtue of their small interaction length probe light-matter interactions over a dynamic range often inaccessible by other optical techniques. They can be used to study biomolecular dynamics of protein folding, catalysis, light harvesting, ion channels and membranes; dynamic processes which can span a range from less than 10^{-9} to more than 10^{3} seconds.[1] Their small size enables an exceedingly high sensitivity, and the application of quantum optical measurement techniques can allow us to approach or surpass classical limits of detection. Quantum photonic micro- and nanosensors may emerge that probe molecules with a sensitivity and resolution far beyond the current state of the art by using quantum correlated nonclassical sources and measurement schemes.[12] By virtue of different materials and geometries, micro- and nanofabricated devices exploit different light-matter interactions with the same analyte molecule. The micro/nanosensor might allow simultaneous access to multiple aspects of the dynamics of single molecules by probing using various wavelengths, different polarizations and intensities of light. The fast transduction or mixing of these optical signals allows for novel spectroscopies and pump-probe detection schemes. It may even become possible to realise a longstanding dream of biologists and biotechnologists of gathering all this information to visualise protein dynamics with atomic resolution.

Already now, micro and nano-sensors have reached a sensitivity-level that allows for the detection of very small single-molecules.[13, 14] These extreme advances in label-free optical detection were first made possible by enhancing the interactions of light with molecules on metal nanostructures. First demonstrations of plasmon-enhanced single-molecule sensing utilised gold nanorods for detecting larger protein molecules in solution, for example streptavidin with a MW~ 53 kDa.[15] The most recent, most dramatic sensitivity enhancements down to single ions, however, were made possible by combining the plasmonic nanoparticle sensors with optical microcavity detection systems.[16] The idea of the resulting optoplasmonic sensors is to enhance the detection signal via the application of the optical microcavity, similar to two micro-mirrors reflecting light and creating multiple cavity passes, i.e cumulative enhancement of the detection signal by a high quality factor of the microcavity. At the same time, the light is focussed, via a metal nanoparticle, down to sub-wavelength scales to overcome the diffraction limit and probe single molecules and ions.

All of the emerging single-molecule sensor systems, optoplasmonic, nanophotonic, or plasmonic, are enabled by advances in micro and nanofabrication. Advances in measurement methodology, laser interferometry, and quantum optics further contribute to the rapid progress of the field. It is this convergence of previously quite disparate fields of scientif ic investigations that is accelerating the recent advances in micro and nanosensing. For researchers entering this rapidly advancing field there is an urgent need for a timely review that covers the most recent developments, one that identifies the most exciting opportunities. The focus of this review is to provide a summary of the recent techniques that have either demonstrated label-free single-molecule detection or claim single-molecule sensitivity. We structure our review into the following sections of: 1. Plasmonic, microcavity, and optoplasmonic label-free sensing approaches; 2. Photonic crystal based sensors; 3. Recent developments in single-molecule plasmon-enhanced label-free optical spectroscopy; and 4. Methodology and recent advancements in quantum photonic sensing in general and its wide possibilities extending to molecular level biosensing. It is pertinent to note that unlike the established single molecule biosensing approaches

reviewed in first three sections, the quantum photonic sensing is still in its infancy. Given the recent fast developments in quantum metrology and communication, quantum photonic sensing is promising in terms of its nonclassical approach to overcome the classical limits in conventional optical sensing schemes. The review closes with an outlook section that identifies some challenges to overcome for these sensors to become widely used in biology and clinical diagnostics. We also identify some exciting applications of label free optical single-molecule sensors. It should be noted here that our aim is not, however, to provide a comprehensive account of all the advancements that have led to the current progress in label-free single-molecule sensor technology. Instead, we would like to refer the readers to other focussed reviews on plasmonic sensing,[13] label-free single-molecule imaging,[17] optical microcavity based sensing,[18, 19] photonic crystal sensors,[20] and Surface-enhanced Raman scattering[21, 22] for a more detailed treatment of the techniques highlighted in this paper .

1. Plasmonic, microcavity, and optoplasmonic label-free sensing approaches

Some of the most recent breakthroughs in optical label-free single molecule sensing can be mainly attributed to the advances in utilization of plasmonic and optical resonators. In general terms, a resonator is a structure that allows only oscillations of a certain 'resonant frequency' to be sustained within. More importantly, this provides for an amplification of the amplitude of the oscillation at this resonance frequency relative to the rest. The resonance frequency is dependent on the properties of the material, the surrounding medium and geometry of the resonator. For example, a tuning fork is an acoustic resonator which oscillates at one particular tone depending on the length and mass of the fork. In the optical domain, similar structures that confine light only of particular frequencies can be fabricated using different materials. These can be broadly classified into two categories, plasmon resonators using metal nanostructures and optical micro- and nano- resonators using dielectric materials. The interaction of an analyte such as biomolecules with the resonator results in a change to the spectral properties of the resonator. These changes are monitored to infer information on the molecule. This mechanism has been successfully exploited to achieve label-free detection of single molecules. In this section, we will highlight the plasmonic,[13, 14] microcavity,[18, 19] and optoplasmonic sensors (a combination of both plasmonic and microcavity sensors)[16, 23] that have very recently enabled the label-free detection of single-molecules.

1.1. Plasmonic sensing approaches

The collective oscillations of the surface electrons in metal nanostructures (where structure size << wavelength of incident light), termed as localized surface plasmon resonances (LSPRs), results in high field localization in very close proximity of a few nm to the nanostructure.[24] The enhancement is extremely high at the tips of rods, stars, and diamonds **(Figure 1A)**. LSPRs can be resonantly excited directly by visible and near infrared light. The scattering of light due to these LSPRs results in the often bright colours commonly seen with solutions of metal nanoparticles. The interaction of chemical and biological species with plasmon enhanced light-fields has been utilized for sensing applications.[13, 25]

LSPRs are a class of morphology dependent resonances, meaning that, the frequency of resonance can be tuned by varying the shape and size of the nanoparticle. The polarizability of the nanoparticle, α, determines the resonance frequency and the extent of the near-field localization, and is given by (with the dipole approximation)[26]

$$\alpha = V \frac{\epsilon_0 \epsilon_m (\epsilon_p(\omega) - \epsilon_m(\omega))}{\epsilon_m(\omega) + L(\epsilon_p(\omega) - \epsilon_m(\omega))} \qquad (1)$$

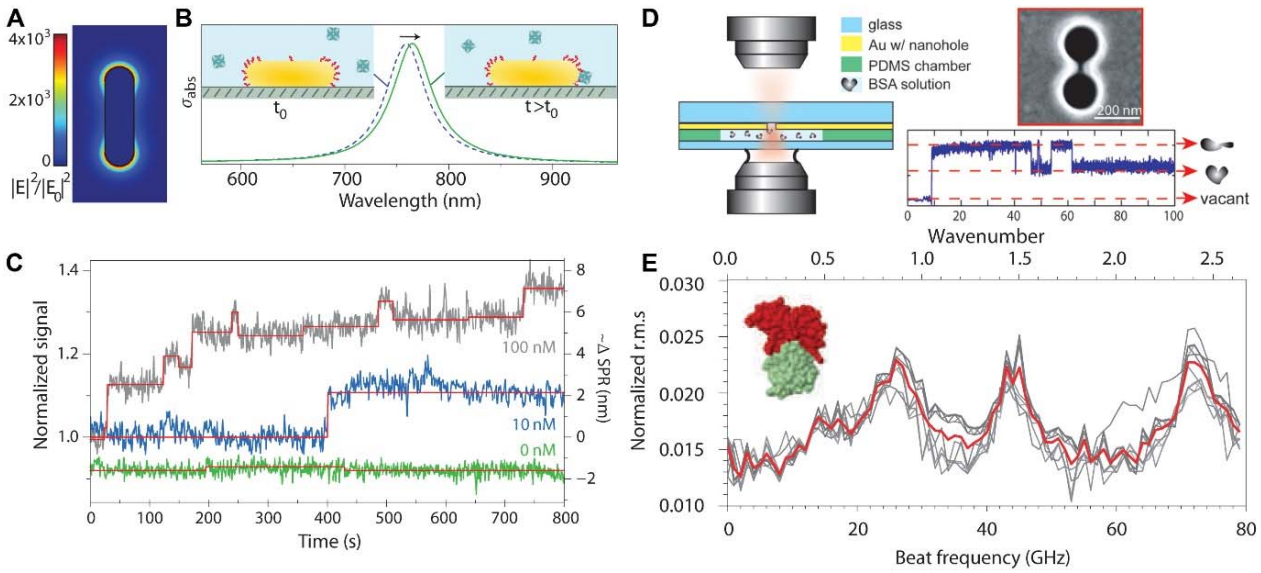

Figure 1. Plasmonic sensing of single molecules. **(A)** Simulation of the near-field of a plasmonic gold nanorod shows an intensity enhancement of the order of 10^3. **(B)** Mechanism of sensing by plasmonic nanorods. The shift of the LSPR resonance peak due to binding of a molecule is monitored. The insets show a sketch of the nanorod at time t_0 where no molecules are attached to the surface, and the time $t > t_0$ where a molecule attaches to the hotspot. **(C)** Time traces of LSPR shift for the binding of streptavidin–R-phycoerythrin conjugate at different concentrations. Adapted with permission.[13] Copyright 2012, Springer Nature. **(D)** Figure shows the double nanohole optical traps for single molecule sensing. The nanohole is a dumbbell shaped structure milled in a gold film coated on a glass substrate. A laser beam is focussed

onto the structure and the transmitted light is collected and captured by an avalanche photodiode. The example trace in subfigure shows step events in the transmission signal due to trapping of a single BSA molecule. Adapted with permission.[27] Copyright 2012, American Chemical Society. **(E)** Low frequency Raman spectrum of a single Conalbumin protein measured as the root mean squared fluctuation of the transmission signal across the optical trap. Adapted with permission.[28] Copyright 2014, Springer Nature.

where V is the volume of the particle, ϵ_0, ϵ_m and ϵ_p are the permittivity of free space, relative permittivites of the surrounding medium and the metal nanoparticle, respectively and L is a shape dependent factor. It is seen from Equation 1 that the surrounding medium affects the polarizability of the plasmonic nanoparticle. This change in polarizability when a molecule enters the near-field of the nanoparticle (permittivity of the surrounding medium is changed) is employed in the label-free detection of single molecules. The change in α is monitored as a shift in the resonance peak position when a molecule interacts with the near-field of the plasmonic nanoparticle **(Figure 1B)**. Using this approach, shifts of the plasmon peak due to the binding of single streptavidin (53 kDa), antibiotin (150 kDa), and a streptavidin–R-phycoerythrin conjugate (300 kDa) to biotin coated gold nanorods **(Figure 1C)** have been reported.[15] This single molecule detection scheme was improved by simultaneously monitoring the scattering from hundreds of nanorods using a dark field microscopy setup.[29] This approach allowed the statistical analysis of antigen-antibody interactions. Although directly observing the LSPR shifts has enabled the detection of single molecules, the signal-to-noise is limited due to the low quality of the resonance.

Instead of monitoring the spectral position of the plasmon resonance, another approach detects single molecules by trapping them using the high field localized around plasmonic nanostructures. The presence of the molecule is detected as a change in the transmission of the illuminating light across the plasmonic structure.[27] The principle of optical trapping is based on the forces acting on a dielectric particle such as a glass bead or a biomolecule due to its interaction with a focussed beam of light. This optical force can be separated into two components, the scattering force and the gradient force.[30] The gradient force acts to pull the particle towards the focal region while the scattering force acts to push it away. Hence, trapping of the scatterer occurs when the pulling gradient force exceeds the pushing scattering force. By confining light into sub-wavelength scales and increasing the local field intensity experienced by a particle, plasmonic nanostructures have enabled trapping of single nano objects,[31] even single proteins.[27] Using a double nanohole structure fabricated on a thin gold (Au) film, trapping of a single bovine serum albumin (BSA) protein could be achieved.[27] The nanohole structure is a dumbbell shaped hole **(Figure 1D)** milled into a thin gold film using focussed ion-beam milling. The structure is illuminated by a focussed laser beam. The optical transmission across the nanohole structure is monitored to detect a trapping event. When a dielectric particle enters the nanohole structure, it changes the refractive index and hence results in a step change in the transmission across the structure **(Figure 1D)**.

Additionally, more information about the molecule can be obtained after the trapping event. The transmission signal also depends on the thermal motion of the molecule in the trap **(Figure 1E)**.[32] This sensitivity to thermal motion of molecules has been used to probe some low frequency (GHz range) vibrational modes of a trapped biomolecule.[28] The principle of detection is based on monitoring the increase in fluctuations of the transmission signal when a vibrational mode of the biomolecule is excited. The excitation is achieved by modulating the electrostriction force (force due to displacement of ions in an external electric field) using an amplitude modulated pump beam. The increased motion of the molecule upon excitation results in an increased fluctuation in the transmission signal across the double nanohole structure. The root mean squared (r.m.s) fluctuation of the transmission signal with varying modulation frequencies provides a vibrational spectrum equivalent to a Raman measurement. In this manner, Wheaton *et al.* could obtain low-frequency Raman spectra for four globular proteins, carbonic anhydrase, conalbumin, cyclooxygenase-2 and Aprotinin.[28] An example spectra for Conalbumin is shown in **Figure 1E**. In subsequent work, theoretically derived Raman intensity spectra were matched with the experimentally obtained low-frequency Raman spectra.[33] In the future, this approach could be extended to high frequency Raman spectra of single proteins as well. However, a few questions such as the smallest size of molecules that can be trapped and if the trapped biomolecules remain functional under the high optical forces in the trap have to be addressed.

1.2. Optical microcavities based approaches

Optical microcavities are structures that confine light into small volumes by resonant recirculation forming optical resonances.[34] These cavities, typically fabricated from dielectric materials such as glass or III-V semiconductors, have a small mode volume, V, and extremely low losses described by a high quality factor, Q. For any cavity, the quality factor, Q, quantifies the temporal confinement of light and is defined as the ratio of energy stored in the cavity to energy dissipated per electromagnetic oscillation, $Q = U(t)/[-\left(\frac{dU(t)}{dt}\right)/\omega_0]$. Here, $U(t)$ is the total energy confined in the cavity and $(-\left(\frac{dU(t)}{dt}\right) / \omega_0)$ is proportional to the energy lost per electromagnetic oscillation and ω_0 is the resonance frequency.[35] From the definition of Q, it follows that the initial energy stored in the cavity decays over time with a time constant, $\tau = Q/\omega_0$. Similarly, the mode volume, V, quantifies the spatial confinement of light. Many definitions are found in literature for the mode volume. For high Q cavities, the mode volume can be defined as the energy density in the mode normalized to the maximum inside it, $V = \int_v (\epsilon(\mathbf{r})|E(\mathbf{r})|^2\, dV)/\max[\epsilon(\mathbf{r})|E(\mathbf{r})|^2\,]$.[34, 36] Here, $\epsilon(\mathbf{r})$ is the permittivity of the material, $E(\mathbf{r})$ the electric field and the integration volume is over the entire space. For sensing applications, the figure-of-merit for a microcavity sensor is given as the ratio of Q/V. Many different cavity structures such as Fabry-Perot cavities, whispering-gallery mode cavities (WGM) and photonic crystal (PhC) cavities have been employed. Among these, WGMs and PhCs are promising due to their ultrahigh quality factors and ultra-small mode volumes, respectively.

Optical WGMs are resonances in dielectric geometries with circular symmetry such as spheroids,[37] toroids,[38] bottles[39], and disks.[40] These resonances are formed when light is trapped due to multiple total-internal reflections at the curved boundary. The term WGM for these optical resonances is obtained from the acoustic analogue. Lord Rayleigh first studied a similar phenomenon for sound waves in St. Paul's Cathedral in London, where the guiding of sound waves in the dome led to whispers being heard from across

the 32-meter gallery.[41] **Figure 2A** shows an illustration of a microsphere cavity where light is trapped due to multiple total internal reflections at the curved interface. The quality factors of these resonances can be extremely high depending on the material and wavelength of light used for the excitation. Ultrahigh quality factor WGM resonators with Q of $10^8 - 10^{10}$ with small mode volumes of $180\ \mu m^3$ have been demonstrated.[42] Although most of the light is confined within the cavity, there exists an evanescent field, hundreds of nanometres long, extending out into the surrounding medium. The interaction of molecules with this evanescent field induces changes to the spectral or scattering properties of the WGM. These changes in the WGM's optical properties is exploited for sensing applications and are monitored using various techniques to extract information about the molecule.[18, 19, 43] The spectral properties can be categorized into three observables; frequency shifts, broadening of the cavity linewidth and mode splitting.[43]

Since biomolecules induce very small losses in the system, the most common mechanism exploited for sensing with WGMs is reactive sensing. The term "reactive" here refers to the change in spectral properties introduced by a purely reactive interaction, that is, by an elastic scatterer which does not induce any absorption losses. In this case, the frequency shifts induced by the analyte are monitored **(Figure 2A)**. The fractional frequency shift of the WGM can be given to the first-order by the simple equation[44]

$$\frac{\delta\omega}{\omega} \cong -\frac{\alpha_{ex}|E(\boldsymbol{r_p})|^2}{2\int_V \epsilon(\boldsymbol{r})|E(\boldsymbol{r})|^2 dV} \qquad (2)$$

Where $\delta\omega/\omega$ is the fractional shift, ω is the resonance frequency, α_{ex} is the difference in polarizability between the molecule and the surrounding medium, ϵ is the refractive index of the cavity medium, $\mathbf{E(r)}$ and $\mathbf{E(r_p)}$ are the electric fields in the cavity and the molecule's position, respectively. In experiment, the fractional shift is acquired continuously either by scanning a tuneable laser over a range around ω or by locking the excitation laser to the cavity resonance frequency (Pound-Drever-Hall lock).[45, 46] Using a tuneable distributed feedback laser (nominal wavelength ≈ 763 nm) and a glass microsphere resonator, single Influenza A viruses could be detected by Vollmer *et al.*[47] Despite the high Q and small V of WGMs, detection of single molecules of small proteins and DNA has not been possible by directly monitoring the frequency shifts of the WGM. A theoretical model by Foreman *et al.* predicts a required enhancement in the frequency shift signal of the order of 10^4 to achieve single biomolecule sensitivity.[48] The straightforward solution to boost the sensitivity is to enhance the field $\mathbf{E(r_p)}$ seen by the biomolecule.[49] This enhancement can be achieved by coupling the WGM to plasmonic nanostructures presented in the previous section. This combination of optical cavities with plasmonic nanostructures has been successfully exploited in optoplasmonic sensors to achieve detection down to single molecules of BSA,[50] study the interactions of single DNA oligomers,[37] monitor the kinetics of single molecule surface reactions[51] and enzyme kinetics,[52] and even monitor interactions of single atomic ions[16] with a gold surface **(Figure 2B)**. Further improvements in terms of signal-to-noise can be achieved by minimizing the errors introduced by laser frequency-jitter and the wavelength sweeping mechanism. These errors can be minimized by either using a reference interferometer to measure the frequency shift[53] or using lock-in detection schemes.[46]

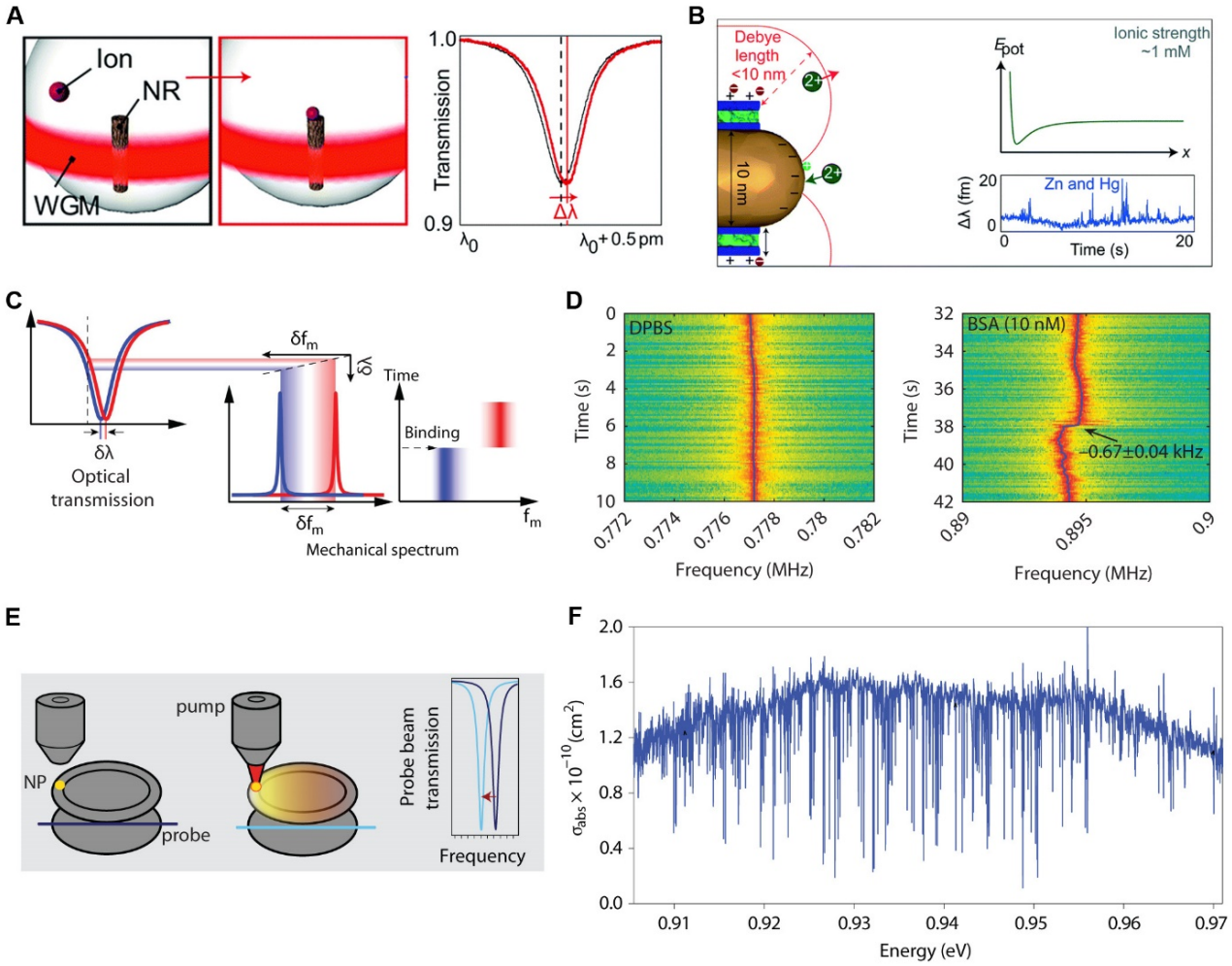

Figure 2. Whispering-gallery mode based single molecule sensing mechanisms. **(A)** Schematic of a WGM-plasmonic hybrid sensor (the gold nanorod is labeled NR in the figure). The WGM field is enhanced by a plasmonic gold nanorod. The analyte, in this case a heavy metal ion, interacts with the gold surface inducing shifts in the WGM resonance peak as depicted. **(B)** WGM shift signals time traces showing two regimes of Zn^{2+} and Hg^{2+} ion interaction with the gold surface. Adapted with permission.[58] Copyright 2017, The Royal Society of Chemistry. **(C)** Optomechanical sensing of single proteins. The WGM shift induced due to BSA binding is translated into a shift in the mechanical mode due to optomechnical coupling of the WGM and mechanical Eigen modes of the cavity. **(D)** Spectrograms showing clear binding steps by individual BSA molecules. Adapted with permission.[54] Copyright 2016, Springer Nature. **(E)** Photothermal absorption spectroscopy of single gold nanorods attached to a toroidal WGM microcavity. Here NP indicates the nanorod. A tuneable modulated pump beam excites the nanorods. The probe beam is coupled into the WGM using a tapered optical fiber. The shift in the WGM resonance due to the photothermal signal is monitored using a Pound-Drever Hall lock-in detection scheme. (F) A fine resolution absorption spectrum obtained by tuning the pump laser from 0.905-0.069 eV. The spikes in the absorption spectrum show Fano features due to the WGM-nanorod coupling. Adapted with permission.[55] Copyright 2016, Springer Nature.

Although combining plasmonics with the WGM enables detection of single molecules, it introduces a few disadvantages. The sensing volume is drastically reduced which might be undesirable for sensing extremely low concentrations of analyte in reasonable timescales of few seconds to an hour. Also, the complexity of the sensor system in terms of assembly is increased with the addition of the plasmonic nanostructure. An approach based on optomechnical coupling of WGMs to the mechanical eigenmodes of the cavity overcomes this issue. The light circulating in a microcavity exerts a radiation pressure on the cavity walls. With the right frequency of light, mutual coupling of the optical and mechanical degrees of freedom of the resonator can be achieved resulting in coherent optomechanical oscillations.[56] This optomechanical resonance frequency and its overtones can be retrieved from the power spectrum of the cavity emission. Due to the coupling of optical and mechanical modes, any shift in the WGMs resonance due to interacting analytes is transferred to a shift in mechanical oscillation frequency. The mechanical resonance peaks can be extremely sharp (sub Hz linewidths) and it possesses a greater shift to linewidth ratio compared to the optical resonance **(Figure 2C)**. In fact, this mechanism has enabled the label-free detection of single bovine serum albumin (BSA) adsorption to a bare silica microcavity. **(Figure 2D)**.[54]

A recently published approach reports single particle photothermal absorption spectroscopy using toroidal whispering-gallery mode cavities.[55] Gold nanorods attached to the surface of a toroidal cavity **(Figure 2E)** are heated using a pump laser with energies from 0.905-0.969 eV (1280-1370 nm). The WGM resonance is excited with a tuneable, narrow linewidth ($\leq$ 300kHz) diode laser

in the wavelength range 1520 – 1570 nm. The WGM resonance is monitored using a frequency lock-in technique (Pound-Drever-Hall lock). Extremely high sensitivity is achieved by amplitude modulation of the pump beam. This allows moving the desired signal into a sub-hertz (0.1375 Hz) band at several kilohertz modulation frequency thus overcoming the low frequency noise contributions. Single particle absorption spectrum of gold nanorods are inferred from the WGM shifts. The coupling of WGM and the nanorod could be monitored with a fine resolution scan of the probe beam, where the Fano line shape of the coupled resonator system could be extracted **(Figure 2F)**. The smallest detected WGM resonance frequency shift with gold nanorods is 84 Hz (1 attometer) corresponding to a power of 20 pW. This power is orders of magnitude smaller than for example photothermal signal of a single dye molecule (order of 10^{-8} W).[57] Although in this proof-of-concept study, plasmonic absorption is used, this approach could be applied to molecular or vibrational transitions as well.[55] More recently, this approach has been applied to studying conductive polymer molecules with the smallest molecules similar in cross-section to single dye molecules.[58] Future single-molecule measurements will have to discriminate, however, the WGM shifts that originate from the heating of single molecules from the WGM shifts that originate from the heating of the surrounding environment by the pump beam, and the heating of the microresonator itself.

2. Photonic crystal based sensors

The ultimate lab-on-a-chip concept, the ability to perform many different tests at the single-molecule level, is a vigorously pursued goal in biosensor research. The desire is to not only achieve improved figure-of-merits for incorporated sensors, such as larger Q-factors or smaller modal volumes, but to move towards miniaturised schemes that are easy to manufacture. A promising candidate for such devices employs Photonic Crystal (PhC) elements[59] for precise light control. These PhCs can be used to produce optical resonant cavities with comparable Q-factors[60, 61] at the micron and nanometer scale, and their fabrication leverages the mature technologies employed in the CMOS manufacturing industry.

At their simplest, PhCs possess a periodic variation in refractive index throughout their body, produced most often by nanostructuring. The periodic environment leads to the constructive and destructive superposition of light waves, forbidding the propagation of some wavelengths of light, and modifying the propagation of others. Analogy is often drawn with electrons in a periodic atomic potential, their wavefunctions interfering to modify the electron transport through the crystal.

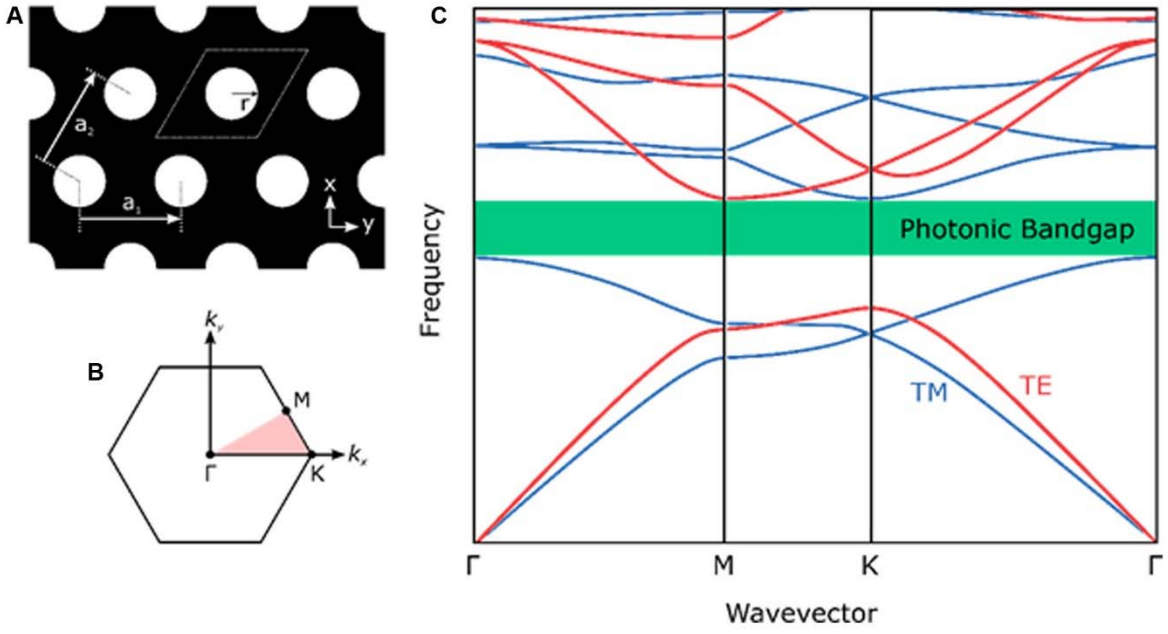

Figure 3. **(A)** An example Photonic Crystal structure consisting of air-holes in a material, possessing a hexagonal lattice with basis vectors a_1 and a_2. The dotted region indicates the primitive cell of the structure. **(B)** The reciprocal space map of the lattice in (A) with the key symmetry points labelled. Adapted with permission. [59] Copyright 2008, Princeton University Press. **(C)** A typical dispersion diagram for the example structure. The allowed light modes that might propagate in the structure are shown as blue and red lines, indicating their polarization state (TM or TE). The region for which no propagating modes exist is shown as a green band.[59] Copyright 2008, Princeton University Press.

Since the analogy of electrons in crystals is so useful, PhC research has borrowed much of the terminology from its electronic counterpart. The dispersion of light through the crystal for various symmetry directions is most often presented as the 'photonic band-structure' of the crystal, plotting the allowed energy (or frequency) against the light's quasi-momentum (or wavevector) states, an example of which is shown in **Figure 3**. Frequency ranges for which light is forbidden to propagate are known as the 'photonic band-gap'. The group velocity of the light is intuitive in such diagrams, as it is simply the gradient of the photonic band. With suitable choice of period, material and symmetry, researchers have demonstrated using PhCs for the negative refraction of light,[62]

subwavelength focussing lenses,[63] self-collimation[64] and even optical cloaking.[65] The possibility of creating such a photonic band-gap via the near-elastic scattering of light in low-loss materials leads to a large density of photonic states at the band-gap. Consequently, designing resonant cavities that utilize surrounding PhC structure for the confinement of light leads to extremely efficient and long-lived resonances, providing the large Q-factors and small modal volumes that are vital for the best biosensors. Creating such a resonant cavity requires the breaking of the otherwise perfect symmetry of an (ideally infinite) PhC structural lattice. Many example and designs of such cavities have been reported; defect cavities,[59, 66] double hetrostructure cavities,[67] nano-slots,[68] and even using designed or intrinsic and unavoidable fabrication imperfections of a PhC structure[69, 70] **(Figure 4)**. Hetrostructure cavities in particular have been shown to produce some of the largest Q-factors,[61] with reports in the literature of up to 11 million, surpassing in Q/V even WGM devices, with typical modal volumes of the order of a cubic wavelength or less.[60]

One instructive example is the 2D PhC waveguide shown in **Figure 4B**. With the possibility of forbidding the propagation of light inside PhCs, waveguides for light can be fabricated using PhCs to confine light to a channel inside a 2D slab. This is achieved by nanopatterning a PhC either side of a channel of bulk material we wish light to travel through. For frequencies (and mode polarisations) that lie within the designed PhC band-gap, the light is confined laterally to the channel by the PhC bandstructure and by total internal reflection perpendicular to the plane of the slab. These waveguide modes that exist in the channel possess their own dispersive characteristics, and can be used to drastically change the light-matter interactions to the benefit of sensing. In particular, near the band-gap edge the group velocity of a waveguide mode can tend towards zero. This

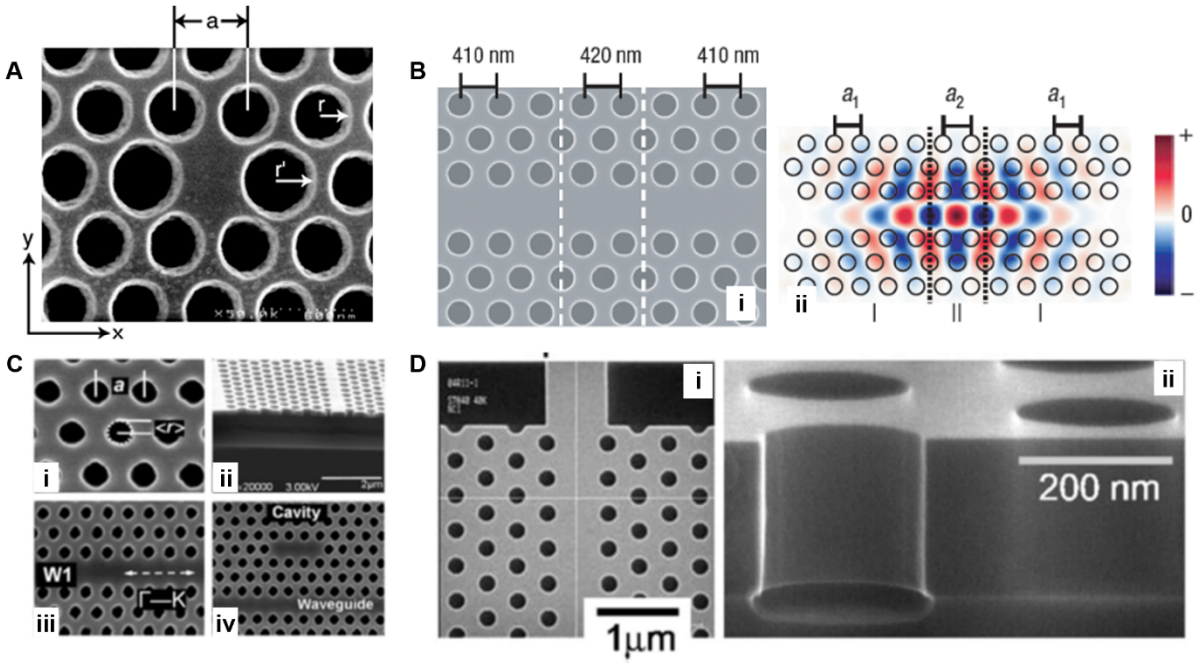

Figure 4. Example PhC resonators. **(A)** Microfabricated 2D hexagonal air hole array in a GaAsP membrane (220 nm thick) used for a defect mode laser device which confines light to 2.5 cubic half-wavelengths, and possess a Q approaching 1500. Reproduced with permission.[71] Copyright 1999, The American Association for the Advancement of Science. **(B)** Scanning electron micrographs of a PhC hetrostructure waveguide. Subtle changes in lattice constant between the dotted lines in (i) allows the confinement of high-Q modes up to 600,000. The electric field profile is also shown in (ii). Reproduced with permission.[67] Copyright 2005, Springer Nature. **(C)** A PhC utilizing the intrinsic fabrication disorder evident in (i) to confine light to random cavities. In this experiment, a 220 nm thick Si slab PhC waveguide (ii, iii) was used to couple in telecomms wavelength light, and measurement of mode lifetimes was achieved by out coupling via a defect cavity show on (iv). These defect cavities themselves can also be efficient resonators. Reproduced with permission.[70] Copyright 2007, American Physical Society. **(D)** An example of a PhC line-defect waveguide used for the characterization of scattering loss from photonic crystal slabs, with the top view (i) and side profile achieved of the holes (ii). Reproduced with permission.[72] Copyright 2005, American Physical Society.

'slow-light' regime results in extremely long-lived and highly confined light-matter interactions. When this slow-light guided mode is coupled with a cavity capable of confining light to a small modal volume, the resulting trapped light may consequently possess extremely large Q-factors that have been reported as high as 10^6.[70]

While three-dimensional PhCs have also been demonstrated,[59, 73, 74] their relatively tricky fabrication with current technology has led to 1D and 2D slab PhCs being the most widely investigated. Since these lower-dimensional geometries are also the most applicable to the future of chip-like biosensors, and so in this review we have restricted ourselves to advances in biosensor technologies employing just these 1D or 2D designs.

With the appropriate PhC cavity and coupling mechanism, various biological analytes have been detected by PhC based sensors. By measuring the spectral resonance shift due to the local change of refractive index in the presence of ensembles of different molecules, PhC structures have been able to detect single-stranded DNA,[75] optically trapped bacteria,[76, 77] ensembles of bovine serum albumin

(BSA) protein,[78, 79, 80, 81] human papillomavirus virus-like particles[82, 83] and multiple NCI-H358 lung cancer cell proteins in lysates.[84] Analyte-specific stoichiometric studies and biomolecule micromanipulation has also been achieved with slotted waveguides,[81, 85] as well as nanobeam cavities.[77, 78, 83, 86] Sub-attomolar detection of steptavidin protein has been reported for PhC nanoslot nanolasers.[68, 80, 87]

Despite PhCs impressive ability to detect biomolecules, single-molecule sensitivity has so far required the addition of a plasmonic element to further concentrate light to a sub-wavelength scale. While novel PhC nanocavities combined with plasmonic nanostructures have emerged as effective hybrid photonic-plasmonic biosensors,[73, 88] biodetection down to the single-molecule level has been claimed to have been achieved so far using nanostructured materials comprising self-assembled silver nanoparticles on PhC diatom biosilica,[89] and has been demonstrated separately in a gold antenna-in-a-nanocavity.[23] These two examples illustrate that single molecule detection using optoplasmonics is possible, but their performance does not represent any fundamental limit of the technology. The results of Laing *et al.*[23] have demonstrated single-molecule level sensitivity by introducing a gold nanosphere inside a 1D PhC waveguide **(Figure 5)**. Using a 50nm gold nanosphere inside a 1D PhC waveguide, Laing *et al.*[23] were able to detect single protein-DNA dynamics with and without the use of fluorescent labels. A key finding in this study showed that interaction between single proteins and DNA was reduced due to electrostatic interactions with the fluorophore, suggesting that label based techniques could be underestimating the rate of protein-DNA dynamics. In the near future, the top-down fabrication methods used in the production of 1D and 2D PhCs should allow the incorporation of more complicated plasmonic resonators to be placed precisely inside PhC resonators, opening the possibility for even higher sensitivities, label-free discrimination and even the determination of the chirality or morphology of a single molecule.

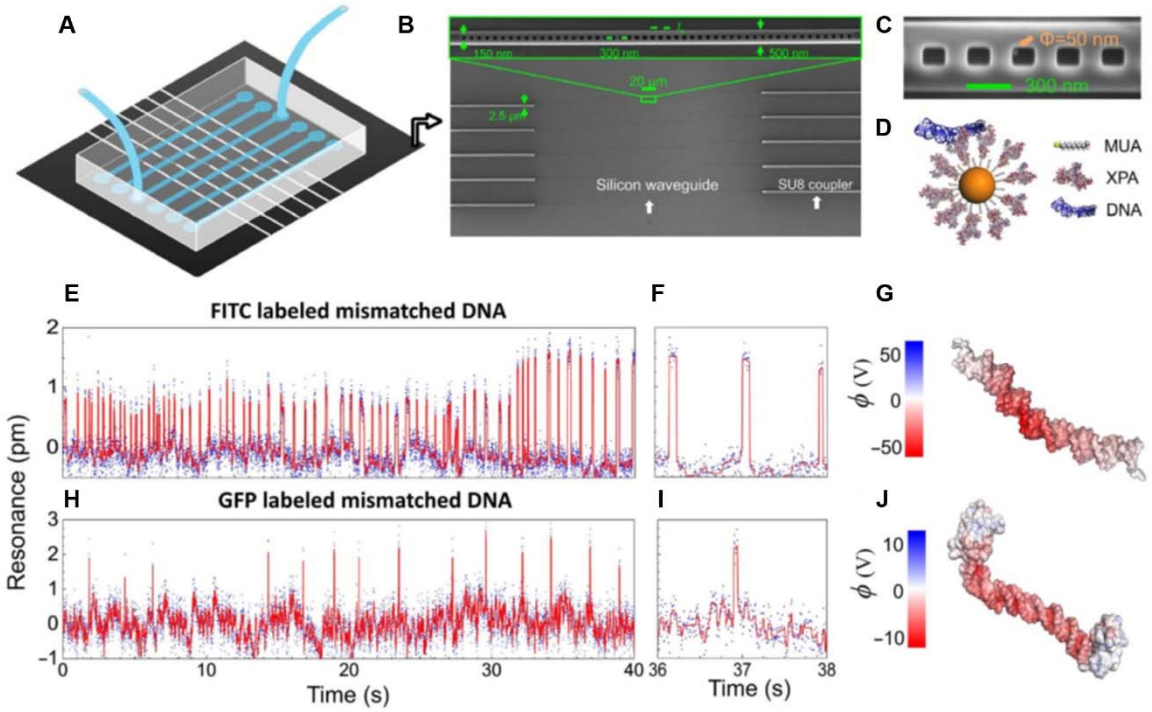

Figure 5. **(A)** Illustration of the PhC sensor system, consisting of the silicon wafer and microfluidics for sample delivery. **(B)** Scanning electron micrographs (SEMs) of the chip shows the multiplexed photonic crystal nanobeam cavities (zoomed inset) connected by waveguiding components for external coupling. **(C)** SEM of the photonic crystal nanobeam cavity, with a single 50-nm-diameter gold particle located in the central nanocavity, forming a plasmonic antenna coupled to the photonic resonator. **(D)** Illustration of the functionalized gold nanoparticle. XPA proteins are immobilized to a self-assembled monolayer of 11-mercaptoundecanoic acid (11-MUA) on gold and interact with a double-stranded DNA (dsDNA). **(E and F)** Real-time binding dynamics of the FITC-labeled mismatched dsDNA and XPA under the standard binding buffer condition, measured from the resonance shifts of the antenna-in-a-nanocavity. **(H to J)** Real-time data for single GFP-labeled dsDNA and XPA protein in the standard buffer (D and E). **(G and J)** The solvent-accessible surface potentials (φ = kBT/e) of a FITC-labeled mismatched dsDNA (G) and GFP-labeled mismatched dsDNA (J). The DNA/dsDNA concentration in the microfluidic channels was 10 nM. Reproduced with permission.[23] Copyright 2017, The American Association for the Advancement of Science.

3. Single-molecule plasmon-enhanced label-free optical spectroscopy

Plasmonic resonances have been exploited in a variety of label-free optical spectroscopic techniques for detection and characterization of molecules. In Raman spectroscopy, for example, the energy difference between the incident and scattered photons, which corresponds to the difference in the quantized vibrational energy levels, yields a unique chemical fingerprint

characteristic of molecules present in terms of their Raman peak positions. Although Raman scattering is a relatively

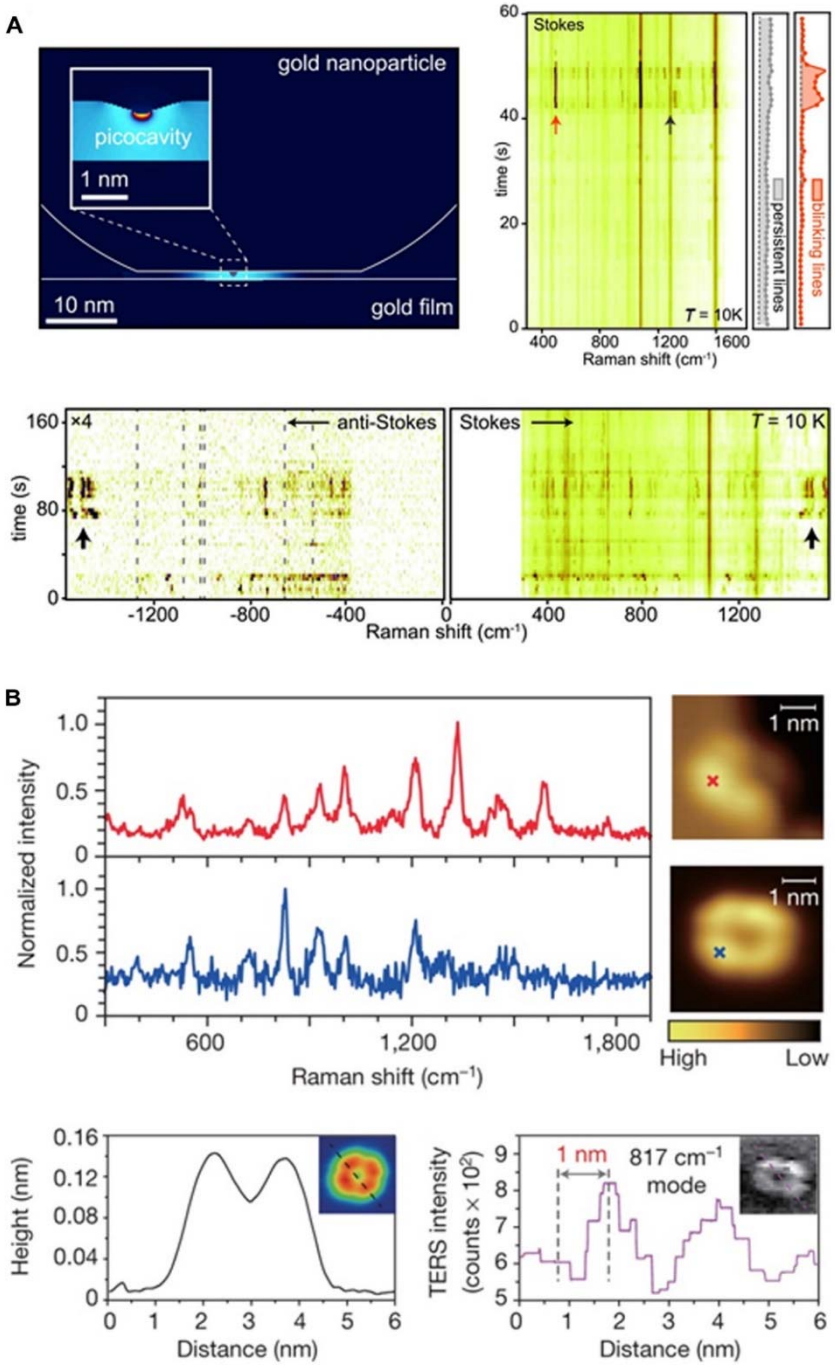

Figure 6. Single-molecule SERS and TERS detection. **(A)** (Top left) Near-field map of a gold nanoparticle on mirror. Inset: zoom-in view of the picocavity showing subnanometer localization of optical field. (Top right) Low-temperature time-series SERS spectra from a gold nanoparticle. Persistent (gray curve) and blinking (red curve) vibrational modes are indicated by black and red arrows. (Bottom) Low-temperature time-series anti-Stokes and Stokes SERS spectra. None of the persistent Stokes modes are seen in the anti-Stokes spectra (dashed lines), and fluctuating anti-Stokes modes appear always and only when the blinking Stokes modes are present (arrows), which is a typical signature of single-molecule SERS. Reproduced with permission.[90] Copyright 2016, AAAS. **(B)** (Top) Representative TERS spectra for a single tilted H_2TBPP molecule adsorbed at the step edge (top, red) and a single flat-lying molecule adsorbed on the terrace (bottom, blue) of Ag(111), both acquired on the molecular lobes marked with crosses shown in the STM images on the right. Subnanometer-resolved STM topograph (bottom left) and TERS mapping (bottom right) for a single H_2TBPP molecule, indicating that the TERS spectral images can provide submolecular information. Reproduced with permission.[91] Copyright 2013, Springer Nature.

weak process, in surface-enhanced Raman spectroscopy (SERS) the extremely high field confinement and enhancement (so-called hot spots) supported by plasmonic nanostructures/nanoparticles enables strong light-matter interactions between localized surface plasmons (LSP) and molecular vibrations. This enhanced light-matter interaction allows for detection of photons emitted by even a single molecule. First observation of single-molecule SERS (SM-SERS) had been reported by two independent groups in 1997.[92] Most work to date on SM-SERS experiments mainly relies on rigorous statistical analysis methods, such as bi-analyte[93, 94] or isotopologue[95, 96] techniques, to unequivocally support the claim of SM-SERS detection sensitivity.[21, 97] In this section, we highlight recent advances in single-molecule plasmon-enhanced spontaneous and coherent Raman spectroscopies in which amplification of the Raman scattering signals is achieved near plasmonic substrate surfaces or within metallic nanoparticle junctions, with emphasis on different technical capabilities.

Plasmonic cavities allow for the subwavelength confinement of light and therefore are often used to enhance light-matter interaction.[98] Benz *et al.* utilized a self-assembled monolayer (SAM) of biphenyl-4-thiol molecules to create a nanometer-thick gap between a gold nanoparticle and a planar gold film.[90] Gold atoms protruding from the surface of the gold nanoparticle are spontaneously formed and destroyed under laser illumination, thus creating plasmonic picocavities, which can be detected by carefully monitoring the blinking of time-dependent SERS signals of the molecules within the picocavity (**Figure 6A**). Since these picocavities are very unstable at room temperature, the authors conducted experiments at cryogenic temperatures. Remarkably such extreme optical confinement enables selective excitation of specific molecular vibrations for different picocavities. The authors were capable of quantifying the population of the excited vibrational states or phonons through the ratio of anti-Stokes to Stokes intensities and extracting Raman localization volume, based on a recently developed quantum mechanical framework that treats SERS in analogy to optomechanical systems.[99, 100] Experimental data clearly show that the optomechanical coupling strength between the picocavity field and molecular vibrations is three to four orders magnitude greater than that of conventional optomechanical systems,[100] setting the basis for developing nonlinear quantum optics on the single-molecule level.

By combining the chemical specificity of tip-enhanced Raman spectroscopy (TERS) with the high spatial resolution of scanning tunneling microscopy (STM) in ultrahigh vacuum and low temperature conditions, Zhang *et al.* successfully developed a novel molecular mapping technique with sub-nanometer resolution. This technique allowed for chemically resolving the inner structure and surface configuration of a single *meso*-tetrakis(3,5-di-tertiarybutylphenyl)-porphyrin (H_2TBPP) molecule that was located within the plasmonic nanocavity formed with the gap between a silver STM tip and a planar silver surface.[91] This unprecedented spatial resolution together with unambiguous chemical identification was achieved mainly by spectral matching of molecular vibronic transitions to nanocavity plasmon resonance which can be tuned by modifying the tip status and changing the gap distance (tunneling current). More importantly, with this technique, the authors were capable of exploring the influence of molecular orientations on the vibrational spectral features (**Figure 6B**). The ability to chemically resolve the internal structure of a single molecule and determine molecular orientation (adsorption configuration) demonstrated in this work has laid the groundwork for future super-resolution, single-molecule chemical imaging studies.[101]

A recent work by Zhang *et al.* demonstrated a single-molecule detection Raman sensitivity through the combination of a Fano-resonant plasmonic substrate and coherent anti-Stokes Raman scattering (CARS).[102] The authors proposed a carefully designed plasmonic substrate composed of a gold quadrumer (four disks) array onto a fused silica substrate (**Figure 7A**). The quadrumer substrate was designed with an anti-bonding dark mode close to the pump wavelength to maximize energy coupling onto the substrate, and broad bonding bright modes spectrally overlapping with the Stokes and anti-Stokes regions to maximize anti-Stokes emission. Interference between the superradiant (bonding) mode, where the dipolar moments of all four disks oscillate in phase, and the subradiant (anti-bonding) mode, where the dipolar moments of the left and right disks oscillate out of phase with that of the top and bottom disks, induces a Fano resonance (sharp dip) in the superradiant continuum at the frequency of the subradiant mode. Both superradiant modes act as optical antennas in this case. Plasmonic nanoantennas have been demonstrated to achieve directional Raman scatterings from single molecules as well as providing enhanced light-matter interactions and controlled far-field radiation patterns.[94, 96, 103] The maximum surface-enhanced CARS (SECARS) enhancement factor (SECARS EF = $g_P^4\, g_S^2\, g_{AS}^2$) was calculated to be ~1.5×10^{10} in the central gap of the quadrumer, as compared to the maximum SERS EF (SERS EF = $g_P^2\, g_S^2$) of ~2.5×10^5, where g is local electric field enhancement ($g = |E(\omega)/E_{inc}(\omega)|$).[104] Experimentally, a Ti:sapphire (76 MHz) laser output was divided into two paths. One path formed an 800-nm pump beam and the other generated a continuum Stokes beam through the use of the nonlinear photonic crystal fiber. The Stokes beam path included a time-delay stage in order to overlap the pulses in time. These two beams were then superimposed spatially using a dichroic mirror. The collinear pump- and Stokes-beams were focused onto an individual gold

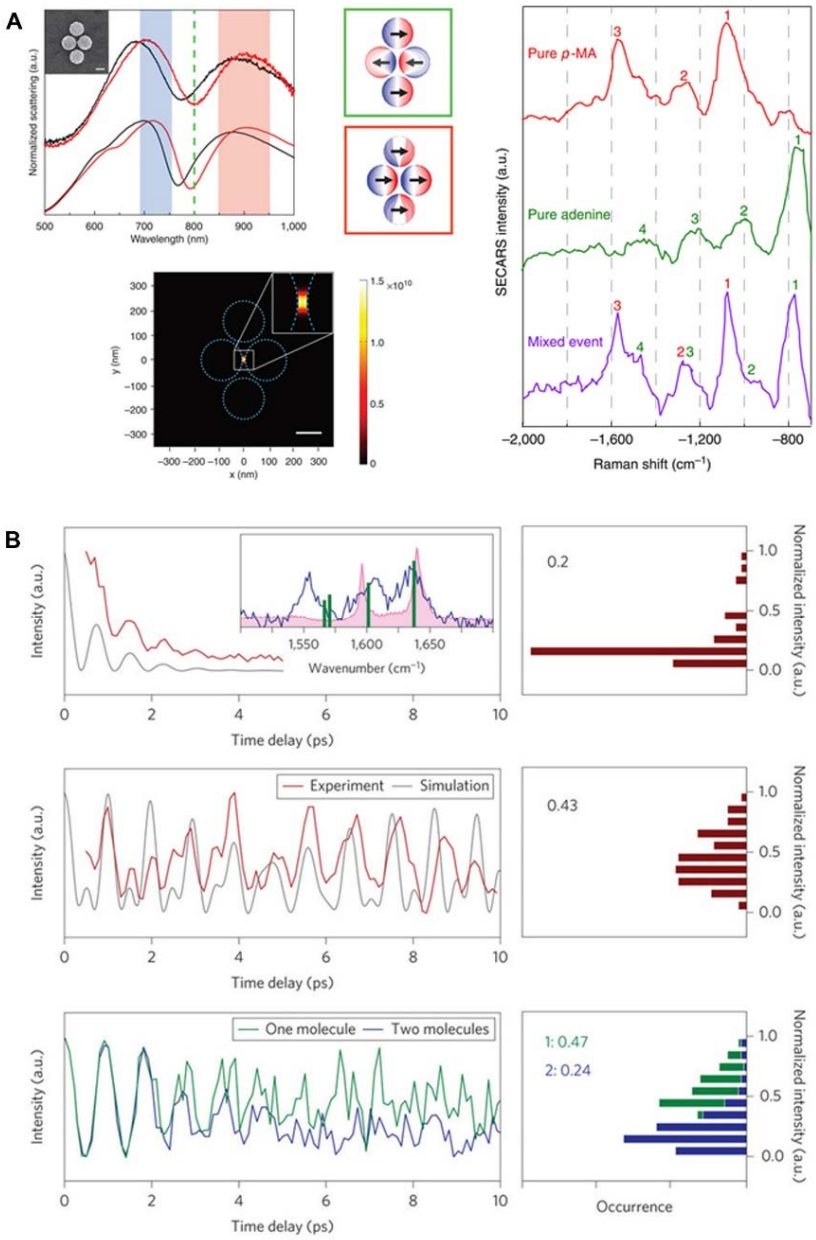

Figure 7. Single-molecule SECARS and TR-SECARS detection. **(A)** (Top left) Measured (top) and simulated (bottom) scattering spectra of a single quadrumer before (black curve) and after (red curve) the analyte absorption. Green dashed line and red/blue shaded zone represent the pump beam and the Stokes/anti-Stokes scattering region, respectively. (Top center) Charge distributions at pump and Stokes frequencies, corresponding to the subradiant (green) and superradiant (red) modes, respectively. (Bottom left) FDTD-computed SECARS enhancement map (bottom left). Scale bar, 100 nm. (Right) SECARS spectra of two individual analytes (red and green curves) and spectrum of both analytes (purple curve), depicting single molecule detection. Reproduced with permission.[102] Copyright 2014, Springer Nature. **(B)** (Top left) TR-CARS signal of bulk BPE (brown curve) and TR-CARS signal retrieved by the windowed Fourier transform of the bulk Raman spectrum (grey curve). Inset shows Raman spectrum of bulk BPE (pink curve) and transient SERS spectrum (blue curve) recorded on the dumbbell. (Middle left) Experimental (brown curve) and simulated (grey curve) TR-SECARS signals of a single dumbbell structure showing distinct quantum beats. The grey curve is a stimulated TR-SECARS response based on the green stick spectrum in the inset. (Bottom left) Simulated TR-SECARS signals for one molecule (green curve) and two molecules (blue curve). (Right) Corresponding PDFs and first moments of the PDFs, showing a single molecule behavior indicated by the first moment of ~0.5. Reproduced with permission.[105] Copyright 2014, Springer Nature.

quadrumer by a 50x/0.8NA objective, and SECARS signal was collected by a 60x/0.7NA objective in a transmitted direction and then analyzed with a spectrograph. To verify single-molecule detection sensitivity, the authors conducted bi-analyte experiments using *para*-mercaptoaniline (*p*-MA) and adenine, and performed their adsorption isotherm measurements to ensure that the difference in the binding affinities of the two analytes didn't affect the statistics.

Using gold nano-dumbbells functionalized with adsorbed *trans*-1,2-bis-(4-pyridyl) ethylene (BPE) and encapsulated in a silica shell as SERS-active aggregates,[106] Yampolsky *et al.* reported a new breakthrough in time-resolved SECARS (TR-SECARS). Their system allowed for real-time observation of the vibrational motion of single molecules through tracking of coherent wave packets sustained on single molecules.[105] The dumbbells were spin-cast from solution onto a silicon nitride membrane substrate, and examined by a nonlinear optical microscope system. Experimentally, a tunable beam (500-750 nm, 170 fs, 80 MHz) from an optical parametric oscillator (OPO) was split into a pump and a probe beam by a beam splitter, and a fixed 809-nm beam (150 fs, 80 MHz) was employed as a Stokes beam in TR-SECARS measurements. The probe beam path included a time-delay stage, and the time-adjustable probe beam was spatially overlapped with the collinear pump/Stokes pulse pair by a dichroic mirror. All three beams were collinearly sent into the microscope system. Through tuning the wavelength of the pump/probe beam and the time delay between the pump/Stokes pair and the probe pulse, the authors were able to show spectrally-resolved TR-SECARS of a single dumbbell acquired under on-resonance and off-resonance conditions. They were also able to observe a signal that oscillated in time in both the forward and backward scattering directions owing to quantum beats. The TR-CARS signal from bulk BPE rapidly dephases in time while the TR-SECARS signal from a single gold dumbbell persists for the 10 ps duration of the measurement (**Figure 7B**), which means that the vibrational coherence on a single nano-antenna is not strongly perturbed by near-field enhancement. This indicates the potential of detection of the coherent wave packets at the single-molecule level. More importantly, the authors were able to show the relationship between the oscillatory TR-SECARS trace and the number of molecules being probed as well as the number of vibrational modes being excited, through the examination of the early-time probability distribution function (PDF) of the signal.

The combination of plasmonic nanomaterials (metallic substrates/tips/nanoparticles) with the inherent chemical selectivity of Raman spectroscopy has become a well-established technique for characterizing molecular interactions in nanoscale environments. High chemical specificity with the capability of high-resolution imaging provided by this technique makes it a unique and effective tool for investigating the dynamics of single-molecule chemical reactions on the nanometer scale. SM-SERS and SM-TERS works, described in this section, were conducted in low temperature condition in order to maintain stable structures and suppress molecular diffusion/desorption and thermal drift problems. The ability to produce robust, reproducible plasmonic nanostructures with controlled placement of molecules directly within uniform and well-defined hot spots makes it possible to systematically investigate single-molecule behaviors and surface-adsorbate interactions under ambient conditions. The coherent nature of ultrafast SECARS and TR-SECARS can, in principle, offer higher sensitivity than spontaneous SERS because SECARS EF scales as g^8 while SERS EF scales as g^4 .[102, 104, 107] Care should be taken to avoid sample degradation when using high irradiance beams with extremely short pulses. Careful control of repetition rate, pump fluences and irradiation times is necessary to routinely acquire spectra with pulsed excitation. Although both g^4 and g^8 laws have been verified experimentally,[102, 104, 108] developing a solid theoretical framework to explore the quantum mechanical nature of the coupling between plasmonic resonances and molecular vibrations and applying the model to interpret observed single-molecule behaviours are required in future investigations of label-free single-molecule vibrational sensing.

4. Quantum photonic sensing: Towards nonclassical fundamental limit in sensing

The coherent control over light-matter interactions at the single photon level has been a driving force as well as a puzzling challenge at the same time for quantum information science and technology.[109] Quantum optical sensing capitalizes on this challenge in order to bring about a paradigm shift and take the sensing protocols to a nonclassical fundamental limit. Quantum sensing protocols widely make use of the recent rapid advancements in the emerging fields of quantum communication, computing and metrology.[110] As mentioned in the introduction, the single molecular-level biosensing by means of quantum optical sensing schemes is still in its infancy. But in order to highlight the promise of quantum photonic sensing and device integration to take the label free sensing to unparalleled detection beyond the classical limits, we briefly outline some of the recent advancements[12, 110] and concepts that dictate their underlying quantum principles in this section. We give a short glimpse on how the sensing scenario could be improved at its fundamental limit by quantum photonic sensing by incorporating nonclassical light sources as well as quantum optical measurement schemes for biochemical sensing in conjunction with nanophotonic and nanoplasmonic sensing techniques.

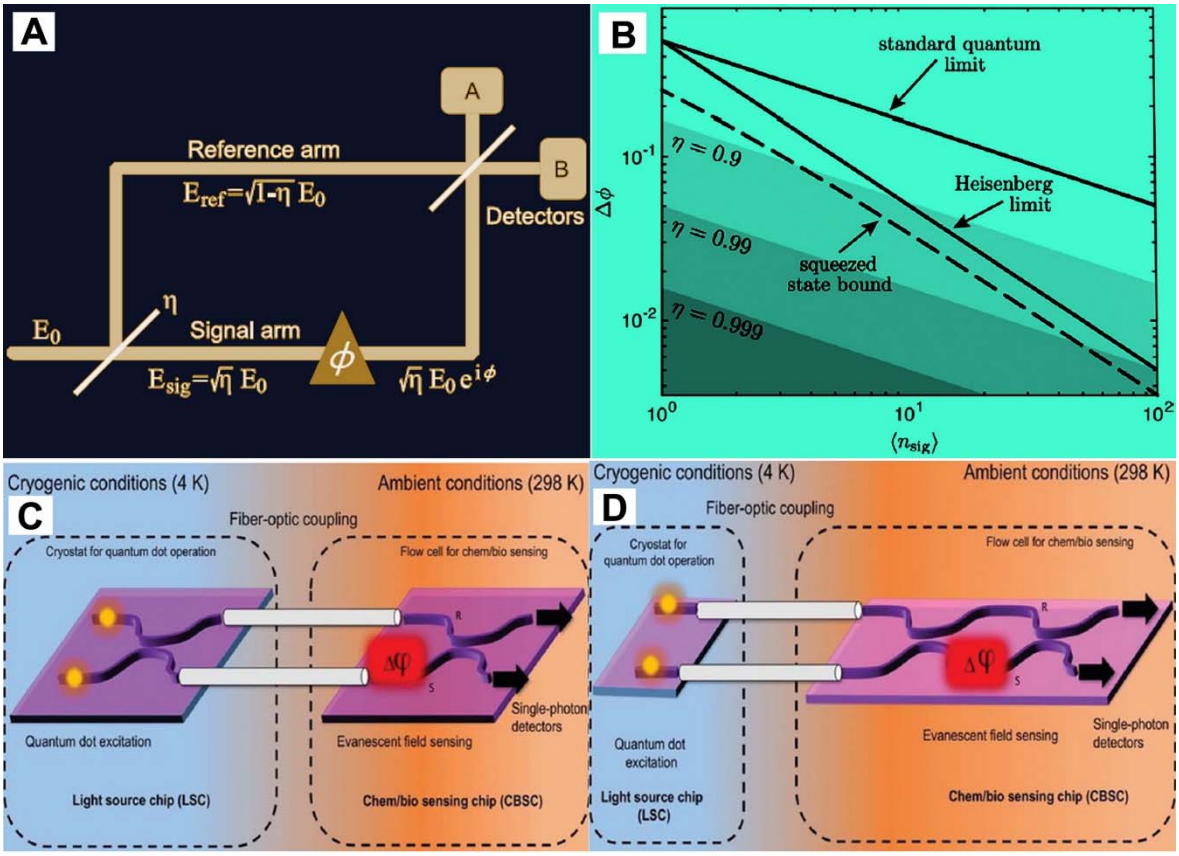

Figure 8. **(A)** Schematic representation of a phase sensing experiment based on a Mach–Zehnder interferometer (MZI). E_0 is the input optical field which is split into reference and signal arm as E_{ref} and E_{sig} respectively. η is the optical transmission of input port beams splitter and φ is the added differential phase. The detection of the output fields at the second output port beam splitter gives the estimated phase shift. Reproduced with permission.[12] Copyright 2015 Elsevier B.V. **(B)** Graphical representations of sensitivity limits of the interferometric phase measurement as a function of mean number of photons $\langle n \rangle$ used. Reproduced with permission.[12] Copyright 2015, Elsevier B.V. **(C)-(D)** Schematic representation of a conceptual design of an integrated nonclassical source chip of entangled photons and a molecular level sensing chip within the scheme of a MZI. Evanescent field sensing in one arm would enable the interaction of the photons in one arm with the analyte molecules at the surface of the waveguide. Reproduced with permission.[111] Copyright 2018, The Royal Society of Chemistry.

Quantum photonic science and technology is envisaged to bring about unprecedented ultra-sensitive detection schemes to overcome the standard quantum limit (SQL) by means of quantum correlated light sources and metrology.[12] The SQL quantifies the best precision achievable in measurement without the use of quantum correlations of photon flux especially for any optical phase measurement.[112] In the meantime, they also have scientific and technological challenges to overcome for them to be compatible with the present day integrated nanophotonic/nanoplasmonic sensing platforms.[112] In 1981, Caves proposed the quantum noise reduction highlighting its importance in optical interferometry.[113] In the recent past, nonclassical sources are getting more attention as promising sources for quantum noise reduction. Two of the very important quantum states of nonclassical light highly preferred in quantum photon sensing are "squeezed states" and "entangled states".[12, 114] The uncertainty principle imposes a fundamental constraint on the product of amplitude and phase quadrature variances of the optical field.[12] In view of this, squeezed states of light are attained by the redistribution of the observable uncertainty, that is, by reducing the uncertainty in the variance of one quadrature (amplitude or phase) and correspondingly increasing uncertainty in the other (amplitude or phase) resulting in precision enhanced measurements of the desired observable.[12, 110] Photon entanglement on the other hand ensures that the quantum state of a photon generated in an entangled pair or in a group of photons cannot be described independently of the state of the other(s), and so are said to be 'entangled'.

For precision enhanced phase measurements which are mostly used in biological and chemical sensing, the maximally path entangled N photon quantum states, the N00N state is widely used.[111] For N entangled photons in an equal superposition of all being in one of the two possible paths A and B, the N00N state is expressed in general as, $|N :: 0\rangle_{A,B} \equiv \frac{1}{\sqrt{2}}\left(|N,0\rangle_{A,B} + |0,N\rangle_{A,B}\right)$.[12, 111, 114, 115]

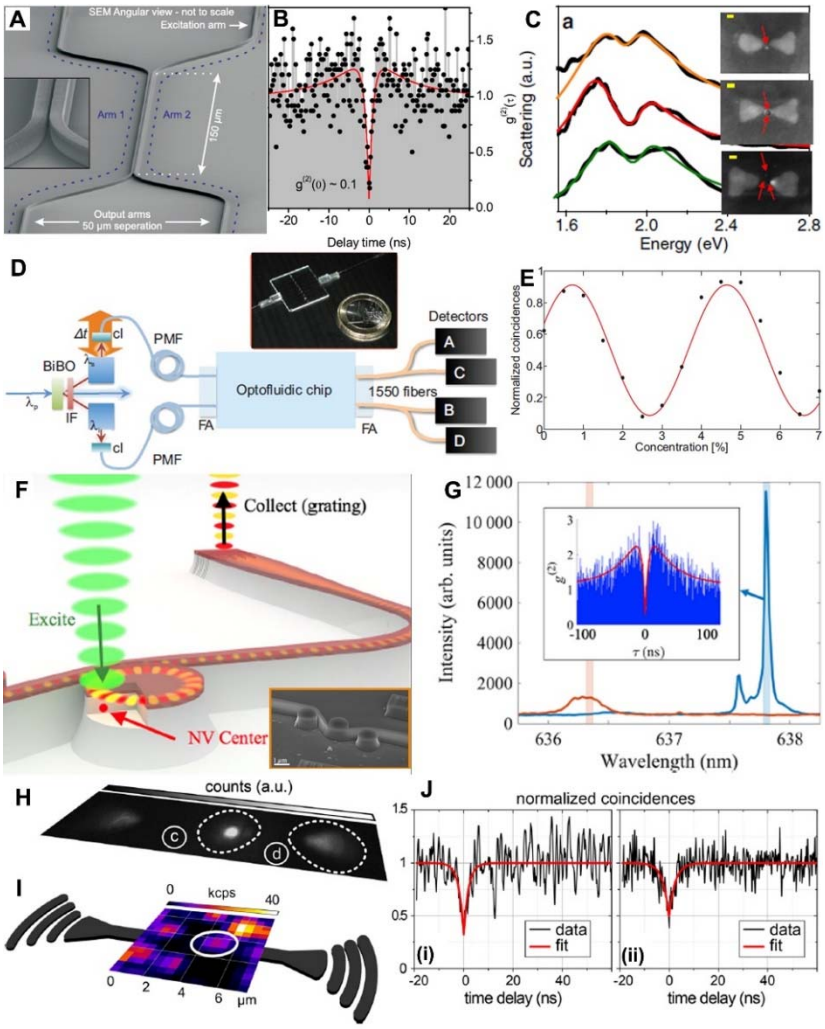

Figure 9. **(A)** Scanning electron micrograph of an on chip beam splitter operating on single photons from quasi-resonantly excited InGaAs/GaAs quantum dots embedded in GaAs rib waveguides. Reproduced with permission.[116] Copyright 2015 AIP Publishing LLC. **(B)** Cross-correlation measurement of the QD emission between both detection arms. Reproduced with permission.[116] Copyright 2015 AIP Publishing LLC. **(C)** CdSe/ZnS QD loaded in to plasmonic bowtie and their scattering spectra showing a transparency dip due to Rabi splitting respectively for (from top to bottom) one, two and three QDs in the gap. Black lines are experimental data whereas the fits to the coupled oscillator model are shown in coloured lines. Insets: SEM images of the bowties where the positions of the QDs are marked by red arrows. Scale bars: 20 nm. Reproduced with permission.[117] Copyright 2016, Springer Nature. **(D)** Schematic representation of an integrated optofluidic device for protein concentration measurement with entangled photons generated in a BiBO nonlinear crystal by SPDC process. Inset: Fabricated device. Reproduced with permission[118] Copyright 2012 American Institute of Physics. **(E)** The measured normalized two photon coincidences for different concentrations of bovine serum albumin in a buffer solution.[118] Copyright 2012 American Institute of Physics. **(F)** Schematic of integrated optical coupling of diamond single NV center to GaP single-mode waveguides. Scanning electron micrograph image of fabricated device in the inset.[119] Copyright 2016 American Physical Society. **(G)** Grating-collected spectra. Blue curve: Cavity tuned onto selected zero phonon line (ZPL) and orange curve: Cavity detuned from ZPL. Photon autocorrelation while cavity is tuned onto ZPL is given in inset.[119] Copyright 2016 American Physical Society. **(H)**-**(J)** Single molecule on chip combing dibenzoterrylene organic molecule-based quantum emitters and dielectric chips consisting of ridge waveguides/grating far-field couplers. **(H)** and **(I)** are respectively the camera image of coupled molecules and the fluorescence confocal scan. Coincidence measurement of coupled nonclassical light showing the antibunching dip relative to the confocal spot (i) and to the coupler area (ii).[120] Copyright 2017 American Chemical Society.

If we consider a Mach–Zehnder interferometer setup as shown in **Figure 8A** incorporating a phase shifter (sample or analyte in real experiments) in signal arm giving an additional phase of $\exp(i\phi)$,[12] it has been estimated that the measured phase for a classical light source will be within the standard quantum limit (SQL) given by $= 1/\sqrt{N}$.[12, 111, 114] Whereas, as shown in the comparative analysis of sensitivity limits of the interferometric phase measurement as a function of mean number of photons in **Figure 8B**, the precision phase measured for a path entangled N00N state nonclassical source would give rise to Heisenberg limit (HL) given by $\Delta \phi_{HL} = 1/N$.[12, 114, 115] In addition to the generation of path entangled photons, hyper-entangled photon pairs of single photons have also been studied which possess correlations in multiple degrees of freedom. As such, they could exist entangled simultaneously in polarization, spatial mode such as orbital angular momentum, and energy-time.[12, 110, 121]

For integrated sensing applications, the entangled photon pairs generated in nonlinear crystals by the spontaneous parametric down conversion (SPDC) process as well as the single photons generated by quantum emitters such as quantum dots (QD) and nitrogen vacancy (NV) centers for precision sensing applications have received high attention.[12, 122] Quantum dots are ubiquitous quantum emitters comprised of a cluster of $10^2 to\ 10^3$ atoms and they have their typical size ranges from 1 to 20 nm.[123] They possess the characteristic property of quantum confinement arising from their ultra-small dimensions.[124] Correlation studies have proven them to be one of the sought after quantum emitters as nonclassical sources which could be further integrated with nanophotonic/nanoplasmonic platforms (**Figure 9A-B**) for integrated quantum photonic sensing for bio molecules.[123, 124] The photonic environment can be highly influenced by the introduction of inhomogeneity and thereby the local density of optical states gets altered.[59, 117, 125] This gives a great boost in the field of integrated quantum plasmonic sensing. One of the interesting fields of investigations is quantum plasmonic sensing, where the sensing platform simultaneously takes advantage of both the quantum nature of light and its electromagnetic field confinement performance by means of a plasmonic interferometer that can beat the standard noise limit.[126] As elaborated in the beginning of this section, entangled photon pairs are anticipated to have a strong impact in the phase measurement sensitivity enhancement in biochemical sensing.[118, 127] One of the demonstrated integrated optofluidic devices for protein concentration measurement with entangled photons generated in a BiBO nonlinear crystal by SPDC process is shown in **Figure 9D-E**.

The luminescent individual point defects in solids such as nitrogen vacancy (NV) centers or color centers in diamonds are atomic-sized quantum photonic nanoscale systems where in general the defect consists of a nitrogen atom replacing a carbon atom and a neighboring lattice vacancy providing a photostable fluorescence in red and IR spectral range of about 100 nm.[128] As they are considered to be solid-state sources of single photons, NV centers form yet another choice of nonclassical light sources for miniaturized integrated quantum optical nanosensing applications.[128, 129] Integrated GaP-on-diamond disk resonators which resonantly couple zero phonon line photons from single NV centers to single-mode waveguides has been demonstrated as shown in **Figure 9F**.[119] The second order correlation measurement performed on the fabricated device showed dips with $g^{(2)} < 0.4$ indicating that maximum number of the collected photons are from a single emitter (**Figure 9G**).[119] Recently Lombardi *et al.* demonstrated a photostable single molecule on chip device combing dibenzoterrylene organic molecule-based quantum emitters and dielectric chips consisting of ridge waveguides/grating far-field couplers.[120] The fabricated molecular nanodevice and the single photon analysis and coincidence measurements are shown in **Figure 9H-J**. As shown in **Figure 10A-D**, the squeezed-light-enhanced mapping of spatial structures within a cell (saccharomyces cerevisiae yeast cell) has been studied observing length scales down to 10 nm. The controlled measurements in water confirmed that, nonclassical squeezed light provides 14% enhancement over the resolution possible with classical coherent light source.[130, 131] Following the investigations to overcome the quantum noise limit in dynamic biological experiments by means of quantum correlation measurements,[12, 132] recently Mauranyapin *et al.* realized an evanescent single biomolecule (bovine serum albumin and anti- Escherichia coli) label-free sensor based on an optical nanofibre operating at the fundamental precision limit dictated by the quantization of light **(Figure 10E-I)**.[133] The study enabled not only the fundamental quantum noise-limited tracking of single biomolecule as small as ~3.5 nm, but also opened the frontier for monitoring the surface–molecule interactions over extended time periods.

5. Outlook

Maturing technology areas such as plasmonics, micro- and nanophotonics, and quantum photonics have arrived at a crossroad. With recent advances in micro/nano fabrication and optical materials, they can soon all be realised on single chip-scale devices. The merger of the previously often disparate areas of technology can shatter the long-standing limits of detection. It was previously argued that the established fields such as plasmonics have fully matured,[134] prompting suggestions that it is now time to do away with metals entirely and explore micro/nanostructures composed only of dielectrics.[135] Although this may be a good idea, we hope that our review identifies another route to break new grounds, by combining the field of plasmonics with the field of dielectric optical microcavities. In certain cases this optoplasmonic approach[14] can take advantage of the best of both fields, as demonstrated for single-molecule sensors with unprecedented levels of detection sensitivity such as single ion sensing.[16] Applying quantum optical measurement techniques to current sensing techniques might further enhance detection sensitivity as demonstrated by the evanescent sensing of single molecules using a tapered optical fiber.[133] Perhaps these and other hybrid sensors can advance much beyond the current state of the art, to realise sensing and spectroscopy of single molecules on a single sensory platform, at room temperature, and with high-throughput. These sensory platforms may be able to characterise Raman modes to discern correctly folded from misfolded proteins in solution, they may identify post-translational modifications and their variations among proteins from single-molecule Raman modes, they may sequence single DNA molecules and identify epigenetic marks on our DNA; ultimately they may visualise the three-dimensional structure of macromolecules at atomic resolution and with a nanosecond time resolution.

Various challenges need to be overcome in the technology areas that we have reviewed for single-molecule micro- and nanosensors in order to achieve these breakthroughs. A few key parameters for to aim for are: varied size range of molecules from single ions to large proteins with sizes of hundreds of kDa, high time resolution, high throughput, specificity of detection in complex media and parallelized detection with many sensors simultaneously. The sensitivity of detecting label-free single molecules using plasmonic nanoparticles is currently limited to a LSPR shift of about 0.5 nm (approximately 1% of linewidth).[13] Hence, the shot noise limited detection limit for single molecules is about 50kDa with just plasmonic nanostructures.[15] Combing optical microcavities with plasmonic sensors is one way to circumvent this issue, where sensitivities to detect single ions have been reported.[16] The maximum size of a molecule detected with plasmonic and optoplasmonic sensors is also restricted due to the decreasing overlap of the molecule and the near-field with increasing molecular size.[15] New nanoparticle structures have to be explored to tune the interaction length to achieve increased enhancements. One advantage of using just plasmonic nanostructures is that they allow for a highly parallelized detection.[29] A parallelized detection scheme has not yet been demonstrated for label-free single-molecule sensing using optoplasmonic sensors. The technical challenges of fabricating a large array of microcavities on chip and combing them with plasmonic structures has to be overcome. Planar micro/nanocavities based on PhCs which can be fabricated using standard cleanroom

technologies might bridge this gap.[23] They might also enable easy integration with novel microfluidic systems to obtain integrated lab-on-chip- devices.[136] Alternatively, single-molecule sensing using bare micro/nanocavities reduce some complexity with assembling optoplasmonic sensors. However, further improvements to the figure-of-merit Q/V have to be achieved.

One of the key advantages of these optical sensors is the high time resolution they offer. This high time resolution will enable accessing the dynamic information of single molecules over varied timescales from nanoseconds to hours. Although most optical label-free single molecule detection schemes so far have reported a time resolution in the millisecond range [15, 23, 37], high speed acquisition in the nanosecond timescale is achievable.[137] The time resolution can be even pushed to picosecond scales with the trade-off being one between the quality factor, Q, of the cavity and time resolution. From the definition of Q in Section 1.2, it can be seen that a higher Q results in the light confined longer in the cavity resulting in longer waiting times for extracting the signal. However, the loss in sensitivity for a higher time resolution could be compensated by combing microcavities with novel plasmonic structures.

The single molecule sensing technologies mentioned in this paper have to overcome the challenge of specificity in complex media to be used in clinical and diagnostic applications. The specificity of detection can be improved by surface functionalizing of the sensors with molecules such as antibodies or amine/thiol polymers which bind to their target partners with extremely high specificity.[138, 139] Commonly, a biotin/streptavidin system is used for highly specific interactions. However, the large size of this complex might be detrimental for sensing with the ultra-small detection volumes of these sensors as discussed previously. Aptamers are small DNA/RNA molecules that can form secondary and tertiary structures capable of binding specifically to proteins and other biomolecules.[140] Hence they are increasingly being used as specific tags for detection of biolmolecules. Alternatively, the single molecules can be identified after attachment to the sensor surface using spectroscopy techniques. However, improvements to the spatial mapping capabilities of the spectroscopy techniques have to be achieved to confirm the acquired single molecule spectra. Single-molecule biosensing in complex media is still challenging. Since field enhancement is confined near the sensor surfaces, nonspecific adsorption activity could impede the binding of target analytes to sensor surfaces and mask the signals from bound target analytes. Therefore, the development of an optimized surface functionalization which can not only effectively resist nonspecific binding but also provides abundant sites for the ligand immobilization is required for reliable single molecule detection.

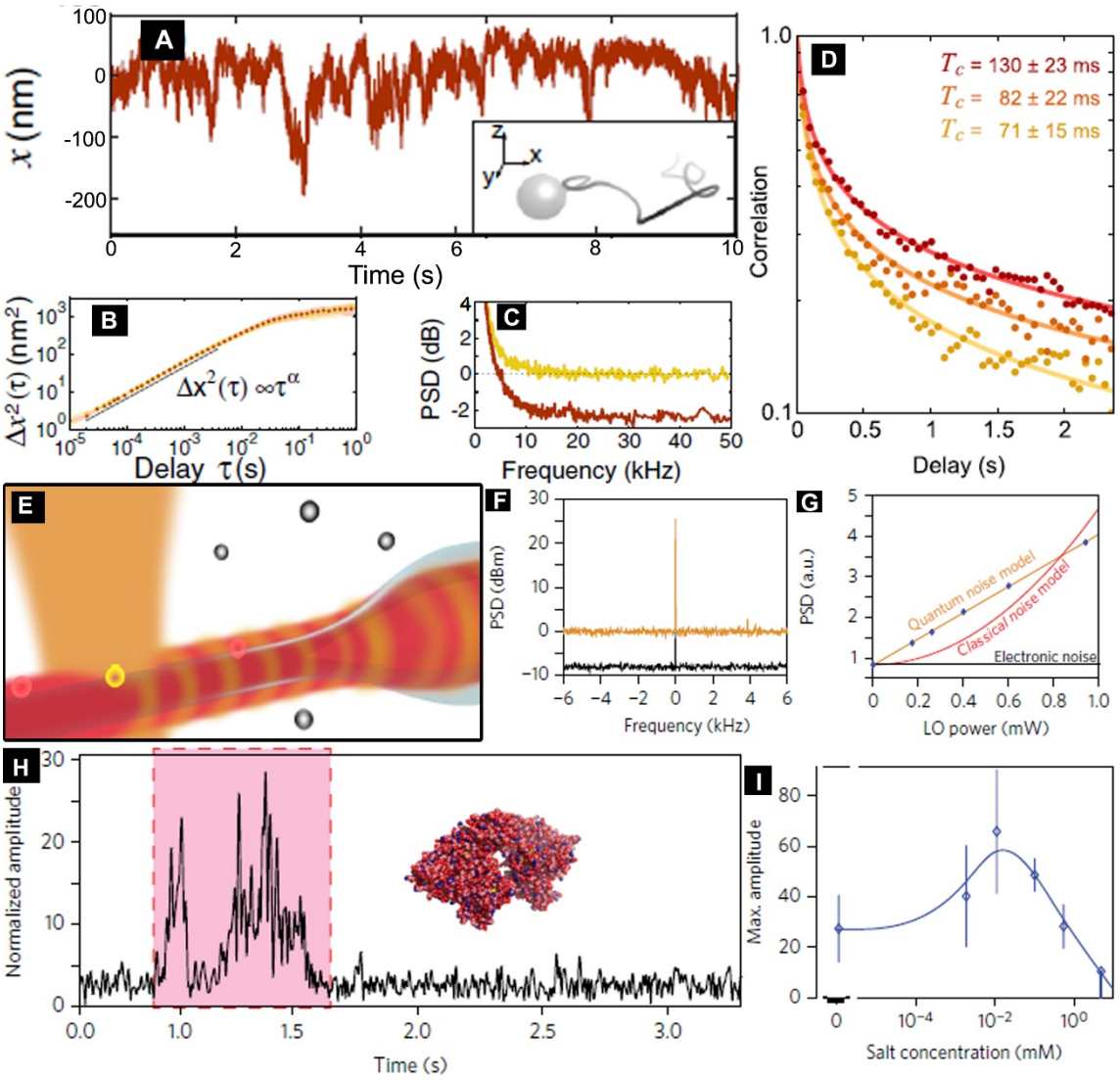

Figure 9. **(A)-(D)** Quantum correlated light-enhanced lipid granule nanoparticle tracking measurements within a living saccharomyces cerevisiae yeast cell.[131] The particle tracking measurement here is based on an amplitude-squeezed local oscillator and an amplitude-modulated probe. Measured particle motion in **(A)** is the x projection of the 3D motion given in the inset. **(B)** Mean-squared displacement (MSD) with both squeezed light (dark red) and coherent light (gold). The diffusive parameter α carries the information about the mechanical properties of the surrounding medium. **(C)** Impact of squeezing is shown by the normalized power spectral density (PSD) plots. The squeezing suppresses the noise floor by 2.4 dB. **(D)** Correlations between sequential measurements of α (x) for three sets of data to verify that the changes in α are spatial, where the estimated T_c is the characteristic time for the particle to diffuse into uncorrelated regions. Reproduced with permission.[131] Copyright 2013, American Physical Society. **(E)-(I)** Evanescent biosensor operating at the fundamental precision limit for quantum noise-limited sensing of single unlabelled biomolecule.[133] **(E)** Schematic of the sensing region of nanofibre with dark-field heterodyne illumination. Nanoparticles (silica naospheres or gold nanorods) in a droplet of ultrapure water are detected when entering the probe beam waist next to the nanofiber as shown in the schematic. The nanofiber biosensor was also subsequently used for the label-free detection measurement of biomolecules as shown (H)-(I). **(F)** The plots of power spectral density (PSD) of the electronic noise (in black) and optical background response (in orange) of the system. **(G)** Averaged PSD over a 10 kHz bandwidth without probe light as a function of the local oscillator (LO) to confirm that the LO field is quantum noise-limited and the electronic noise can be neglected at frequencies above a few hertz. **(H)-(I)** Label-free detection of bovine serum albumin (BSA) biomolecule. Time trace of normalized amplitude for a typical detection event from a solution containing BSA at 0.26 ng ml^{-1} is given in (H). The detection event is highlighted in shaded region. Mean of maximum amplitude of detection events as a function of salt concentration (I), where the total number of observed trapping events at each concentration were 12, 8, 9, 7, 10 and 1. The Stoke radius of BSA was 3.5 nm. Reproduced with permission.[133] Copyright 2017, Springer Nature.

The label-free single molecule sensors presented in this review gain their sensitivity mostly due to high field localization into ultra-small volumes. Hence, relatively large concentrations of analyte are required to get significant detection events in practical timescales of a few minutes. This requirement introduces a constraint on the throughput of these sensors. Integrating these sensors with novel

microfluidic technologies for targeted delivery of the biomolecules to the sensors surface could overcome this issue.[139] Finally, overcoming the above mentioned challenges will lead to integrated sensors that can be deployed in a variety of application areas such as environmental and health monitoring, smart manufacturing, space applications, security, astronomy, robotics, and precision sensing applications.

References

[1] K. Henzler-Wildman, D. Kern, *Nature* **2007**, *450*, 964.
[2] X. C. Bai, G. McMullan, S. H. Scheres, *Trends Biochem Sci* **2015**, *40*, 49; W. Kuhlbrandt, *Science* **2014**, *343*, 1443.
[3] H. M. Berman, *Nucleic Acids Research* **2000**, *28*, 235.
[4] A. G. Kikhney, D. I. Svergun, *FEBS Lett* **2015**, *589*, 2570.
[5] L. E. Kay, *J Magn Reson* **2005**, *173*, 193; I. R. Kleckner, M. P. Foster, *Biochim Biophys Acta* **2011**, *1814*, 942; M. Kovermann, P. Rogne, M. Wolf-Watz, *Q Rev Biophys* **2016**, *49*, e6.
[6] T. E. Wales, J. R. Engen, *Mass Spectrom Rev* **2006**, *25*, 158; J. L. Benesch, B. T. Ruotolo, *Curr Opin Struct Biol* **2011**, *21*, 641.
[7] A. N. Kapanidis, T. Strick, *Trends Biochem Sci* **2009**, *34*, 234.
[8] S. Weiss, *Nat Struct Biol* **2000**, *7*, 724.
[9] X. Michalet, S. Weiss, M. Jager, *Chem Rev* **2006**, *106*, 1785.
[10] C. P. Toseland, *J Chem Biol* **2013**, *6*, 85.
[11] L. Yin, W. Wang, S. Wang, F. Zhang, S. Zhang, N. Tao, *Biosens Bioelectron* **2015**, *66*, 412.
[12] M. A. Taylor, W. P. Bowen, *Physics Reports* **2016**, *615*, 1.
[13] A. B. Taylor, P. Zijlstra, *ACS Sensors* **2017**, *2*, 1103.
[14] J. Xavier, S. Vincent, F. Meder, F. Vollmer, *Nanophotonics* **2018**, *7*, 1.
[15] P. Zijlstra, P. M. Paulo, M. Orrit, *Nat Nanotechnol* **2012**, *7*, 379.
[16] M. D. Baaske, F. Vollmer, *Nature Photonics* **2016**, *10*, 733.
[17] J. O. Arroyo, P. Kukura, *Nature Photonics* **2016**, *10*, 11.
[18] E. Kim, M. D. Baaske, F. Vollmer, *Lab Chip* **2017**, *17*, 1190.
[19] Y. Zhi, X. C. Yu, Q. Gong, L. Yang, Y. F. Xiao, *Adv Mater* **2017**, *29*.
[20] R. V. Nair, R. Vijaya, *Progress in Quantum Electronics* **2010**, *34*, 89.
[21] A. B. Zrimsek, N. Chiang, M. Mattei, S. Zaleski, M. O. McAnally, C. T. Chapman, A. I. Henry, G. C. Schatz, R. P. Van Duyne, *Chem Rev* **2017**, *117*, 7583.
[22] N. L. Gruenke, M. F. Cardinal, M. O. McAnally, R. R. Frontiera, G. C. Schatz, R. P. Van Duyne, *Chem Soc Rev* **2016**, *45*, 2263.
[23] F. Liang, Y. Guo, S. Hou, Q. Quan, *Sci Adv* **2017**, *3*, e1602991.
[24] M. A. Beuwer, B. van Hoof, P. Zijlstra, *J Phys Chem C Nanomater Interfaces* **2018**, *122*, 4615.
[25] J. N. Anker, W. P. Hall, O. Lyandres, N. C. Shah, J. Zhao, R. P. Van Duyne, *Nature Materials* **2008**, *7*, 442; A. G. Brolo, *Nature Photonics* **2012**, *6*, 709; M. Li, S. K. Cushing, N. Wu, *The Analyst* **2015**, *140*, 386; K. Saha, S. S. Agasti, C. Kim, X. Li, V. M. Rotello, *Chemical Reviews* **2012**, *112*, 2739; K. A. Willets, R. P. Van Duyne, *Annual Review of Physical Chemistry* **2007**, *58*, 267.
[26] W. L. Barnes, *American Journal of Physics* **2016**, *84*, 593.
[27] Y. Pang, R. Gordon, *Nano Lett* **2012**, *12*, 402.
[28] S. Wheaton, R. M. Gelfand, R. Gordon, *Nature Photonics* **2014**, *9*, 68.
[29] M. A. Beuwer, M. W. Prins, P. Zijlstra, *Nano Lett* **2015**, *15*, 3507.
[30] A. Ashkin, J. M. Dziedzic, J. E. Bjorkholm, S. Chu, *Optics Letters* **1986**, *11*, 288; K. C. Neuman, S. M. Block, *Rev Sci Instrum* **2004**, *75*, 2787; K. C. Neuman, A. Nagy, *Nat Methods* **2008**, *5*, 491.
[31] M. L. Juan, M. Righini, R. Quidant, *Nature Photonics* **2011**, *5*, 349.
[32] A. Weigel, P. Kukura, *Nature Photonics* **2015**, *9*, 11.
[33] T. DeWolf, R. Gordon, *Physical Review Letters* **2016**, *117*, 138101.
[34] K. J. Vahala, *Nature* **2003**, *424*, 839.

[35] F. Vollmer, L. Yang, *Nanophotonics* **2012**, *1*, 267.
[36] S. Balac, P. Féron, FOTON, UMR CNRS, **2016**; T. J. Kippenberg, in *Engineering and Applied Science*, California Institute of Technology, **2004**.
[37] M. D. Baaske, M. R. Foreman, F. Vollmer, *Nat Nanotechnol* **2014**, *9*, 933.
[38] D. K. Armani, T. J. Kippenberg, S. M. Spillane, K. J. Vahala, *Nature* **2003**, *421*, 925.
[39] M. Pollinger, D. O'Shea, F. Warken, A. Rauschenbeutel, *Phys Rev Lett* **2009**, *103*, 053901.
[40] M. Soltani, S. Yegnanarayanan, A. Adibi, *Optics Express* **2007**, *15*, 4694.
[41] L. Rayleigh, *Philosophical Magazine Series 6* **1910**, *20*, 1001; L. Rayleigh, *Philosophical Magazine Series 6* **1914**, *27*, 100.
[42] M. L. Gorodetsky, A. A. Savchenkov, V. S. Ilchenko, *Optics Letters* **1996**, *21*, 453; T. J. Kippenberg, S. M. Spillane, K. J. Vahala, *Applied Physics Letters* **2004**, *85*, 6113.
[43] M. R. Foreman, J. D. Swaim, F. Vollmer, *Adv Opt Photonics* **2015**, *7*, 168.
[44] S. Arnold, M. Khoshsima, I. Teraoka, S. Holler, F. Vollmer, *Optics Letters* **2003**, *28*, 272.
[45] E. D. Black, *American Journal of Physics* **2001**, *69*, 79.
[46] J. D. Swaim, J. Knittel, W. P. Bowen, *Applied Physics Letters* **2013**, *102*, 183106.
[47] F. Vollmer, S. Arnold, D. Keng, *Proc Natl Acad Sci U S A* **2008**, *105*, 20701.
[48] M. R. Foreman, W. L. Jin, F. Vollmer, *Opt Express* **2014**, *22*, 5491.
[49] M. A. Santiago-Cordoba, S. V. Boriskina, F. Vollmer, M. C. Demirel, *Applied Physics Letters* **2011**, *99*, 073701.
[50] V. R. Dantham, S. Holler, C. Barbre, D. Keng, V. Kolchenko, S. Arnold, *Nano Lett* **2013**, *13*, 3347.
[51] E. Kim, M. D. Baaske, F. Vollmer, *Adv Mater* **2016**, *28*, 9941.
[52] E. Kim, M. D. Baaske, I. Schuldes, P. S. Wilsch, F. Vollmer, *Sci Adv* **2017**, *3*, e1603044.
[53] T. Lu, H. Lee, T. Chen, S. Herchak, J. H. Kim, S. E. Fraser, R. C. Flagan, K. Vahala, *Proc Natl Acad Sci U S A* **2011**, *108*, 5976.
[54] W. Yu, W. C. Jiang, Q. Lin, T. Lu, *Nat Commun* **2016**, *7*, 12311.
[55] K. D. Heylman, N. Thakkar, E. H. Horak, S. C. Quillin, C. Cherqui, K. A. Knapper, D. J. Masiello, R. H. Goldsmith, *Nature Photonics* **2016**, *10*, 788.
[56] M. Aspelmeyer, T. J. Kippenberg, F. Marquardt, *Reviews of Modern Physics* **2014**, *86*, 1391; T. J. Kippenberg, K. J. Vahala, *Science* **2008**, *321*, 1172.
[57] A. Gaiduk, M. Yorulmaz, P. V. Ruijgrok, M. Orrit, *Science* **2010**, *330*, 353.
[58] E. H. Horak, M. T. Rea, K. D. Heylman, D. Gelbwaser-Klimovsky, S. K. Saikin, B. J. Thompson, D. D. Kohler, K. A. Knapper, W. Wei, F. Pan, P. Gopalan, J. C. Wright, A. Aspuru-Guzik, R. H. Goldsmith, *Nano Letters* **2018**, *18*, 1600.
[59] J. D. Joannopoulos, S. G. Johnson, J. N. Winn, R. D. Meade, *Photonic crystals: molding the flow of light*, Princeton university press, **2011**.
[60] T. Asano, Y. Ochi, Y. Takahashi, K. Kishimoto, S. Noda, *Optics Express* **2017**, *25*, 1769.
[61] H. Sekoguchi, Y. Takahashi, T. Asano, S. Noda, *Opt Express* **2014**, *22*, 916.
[62] E. Cubukcu, K. Aydin, E. Ozbay, S. Foteinopoulou, C. M. Soukoulis, *Nature* **2003**, *423*, 604.
[63] E. Cubukcu, K. Aydin, E. Ozbay, S. Foteinopoulou, C. M. Soukoulis, *Phys. Rev. Lett.* **2003**, *91*, 207401.
[64] H. Kosaka, T. Kawashima, A. Tomita, M. Notomi, T. Tamamura, T. Sato, S. Kawakami, *Applied Physics Letters* **1999**, *74*, 1212.
[65] T. Ergin, N. Stenger, P. Brenner, J. B. Pendry, M. Wegener, *Science* **2010**, *328*, 337.
[66] M. Notomi, *Reports on Progress in Physics* **2010**, *73*, 96501.
[67] B.-S. Song, S. Noda, T. Asano, Y. Akahane, *Nature Materials* **2005**, *4*, 207.
[68] S. Kita, S. Hachuda, S. Otsuka, T. Endo, Y. Imai, Y. Nishijima, H. Misawa, T. Baba, *Optics Express* **2011**, *19*, 17683.
[69] L. Sapienza, H. Thyrrestrup, S. Stobbe, P. D. Garcia, S. Smolka, P. Lodahl, *Science* **2010**, *327*, 1352 LP ; J. Topolancik, F. Vollmer, R. Ilic, M. Crescimanno, *Optics Express* **2009**, *17*, 12470.
[70] J. Topolancik, B. Ilic, F. Vollmer, *Physical Review Letters* **2007**, *99*, 253901.
[71] O. Painter, *Science* **1999**, *284*, 1819.

[72] E. Kuramochi, M. Notomi, S. Hughes, A. Shinya, T. Watanabe, L. Ramunno, *Physical Review B* **2005**, *72*, 161318(R).
[73] A. I. Aristov, M. Manousidaki, A. Danilov, K. Terzaki, C. Fotakis, M. Farsari, A. V. Kabashin, *Scientific Reports* **2016**, *6*, 25380.
[74] L. A. Woldering, A. P. Mosk, W. L. Vos, *Phys. Rev. B* **2014**, *90*, 115140.
[75] V. Toccafondo, J. García-Rupérez, M. J. Bañuls, A. Griol, J. G. Castelló, S. Peransi-Llopis, A. Maquieira, *Optics Letters* **2010**, *35*, 3673.
[76] M. Tardif, J.-B. Jager, P. R. Marcoux, K. Uchiyamada, E. Picard, E. Hadji, D. Peyrade, *Applied Physics Letters* **2016**, *109*, 133510.
[77] T. van Leest, J. Caro, *Lab on a Chip* **2013**, *13*, 4358.
[78] Y.-F. Chen, X. Serey, R. Sarkar, P. Chen, D. Erickson, *Nano Letters* **2012**, *12*, 1633.
[79] D. Dorfner, T. Zabel, T. Hürlimann, N. Hauke, L. Frandsen, U. Rant, G. Abstreiter, J. Finley, *Biosensors and Bioelectronics* **2009**, *24*, 3688; M. Lee, P. M. Fauchet, *Optics Express* **2007**, *15*, 4530; N. Skivesen, A. Têtu, M. Kristensen, J. Kjems, L. H. Frandsen, P. I. Borel, *Optics Express* **2007**, *15*, 3169; S. Zlatanovic, L. W. Mirkarimi, M. M. Sigalas, M. A. Bynum, E. Chow, K. M. Robotti, G. W. Burr, S. Esener, A. Grot, *Sensors and Actuators B: Chemical* **2009**, *141*, 13; Y. Zou, S. Chakravarty, D. N. Kwong, W. C. Lai, X. Xu, X. Lin, A. Hosseini, R. T. Chen, *IEEE Journal of Selected Topics in Quantum Electronics* **2014**, *20*, 171.
[80] S. Kita, S. Otsuka, S. Hachuda, T. Endo, Y. Imai, Y. Nishijima, H. Misawa, T. Baba, *IEICE transactions on electronics* **2012**, *95*, 188.
[81] M. G. Scullion, T. F. Krauss, A. Di Falco, *Sensors (Basel)* **2013**, *13*, 3675.
[82] J. E. Baker, R. Sriram, B. L. Miller, *Lab on a Chip* **2017**, *17*, 1570; S. Pal, A. R. Yadav, M. A. Lifson, J. E. Baker, P. M. Fauchet, B. L. Miller, *Biosensors and Bioelectronics* **2013**, *44*, 229.
[83] P. Kang, P. Schein, X. Serey, D. O'Dell, D. Erickson, *Scientific Reports* **2015**, *5*, 12087.
[84] S. Chakravarty, W.-C. Lai, Y. Zou, H. A. Drabkin, R. M. Gemmill, G. R. Simon, S. H. Chin, R. T. Chen, *Biosensors and Bioelectronics* **2013**, *43*, 50.
[85] A. Di Falco, L. O'Faolain, T. F. Krauss, *Applied Physics Letters* **2009**, *94*, 63503; A. H. Safavi-Naeini, T. P. M. Alegre, M. Winger, O. Painter, *Applied Physics Letters* **2010**, *97*, 181106; M. G. Scullion, A. Di Falco, T. F. Krauss, *Biosensors and Bioelectronics* **2011**, *27*, 101.
[86] Y. Chen, W. S. Fegadolli, W. M. Jones, A. Scherer, M. Li, *ACS Nano* **2014**, *8*, 522; F. Liang, N. Clarke, P. Patel, M. Loncar, Q. Quan, *Optics Express* **2013**, *21*, 32306; F. Liang, Q. Quan, *ACS Photonics* **2015**, *2*, 1692; T. Lin, X. Zhang, G. Zhou, C. F. Siong, J. Deng, *Journal of the Optical Society of America B* **2015**, *32*, 1788; T.-W. Lu, P.-T. Lee, *Optics Letters* **2013**, *38*, 3129; X. Serey, S. Mandal, D. Erickson, *Nanotechnology* **2010**, *21*, 305202; G. Shambat, S.-R. Kothapalli, J. Provine, T. Sarmiento, J. Harris, S. S. Gambhir, J. Vučković, *Nano Letters* **2013**, *13*, 4999.
[87] H. Abe, M. Narimatsu, T. Watanabe, T. Furumoto, Y. Yokouchi, Y. Nishijima, S. Kita, A. Tomitaka, S. Ota, Y. Takemura, T. Baba, *Optics Express* **2015**, *23*, 17056; T. Baba, *MRS Communications* **2015**, *5*, 555; T. Baba, S. Kita, H. Abe, S. Hachuda, M. Narimatsu, S. Otsuka, K. Nozaki, in *Active Photonic Materials IV*, Vol. 8095, International Society for Optics and Photonics, **2011**, 80950X; S. Hachuda, S. Otsuka, S. Kita, T. Isono, M. Narimatsu, K. Watanabe, Y. Goshima, T. Baba, *Optics Express* **2013**, *21*, 12815; S. Hachuda, T. Watanabe, D. Takahashi, T. Baba, *Optics Express* **2016**, *24*, 12886; S. Lin, J. Hu, L. Kimerling, K. Crozier, *Optics Letters* **2009**, *34*, 3451; D. Takahashi, S. Hachuda, T. Watanabe, Y. Nishijima, T. Baba, *Applied Physics Letters* **2015**, *106*, 131112.
[88] C. Ciminelli, D. Conteduca, F. Dell'Olio, M. N. Armenise, *IEEE Photonics Journal* **2014**, *6*, 1; F. De Angelis, G. Das, P. Candeloro, M. Patrini, M. Galli, A. Bek, M. Lazzarino, I. Maksymov, C. Liberale, L. C. Andreani, E. Di Fabrizio, *Nature Nanotechnology* **2009**, *5*, 67; F. De Angelis, M. Patrini, G. Das, I. Maksymov, M. Galli, L. Businaro, L. C. Andreani, E. Di Fabrizio, *Nano Letters* **2008**, *8*, 2321; Y. A. Kelaita, K. A. Fischer, T. M. Babinec, K. G. Lagoudakis, T. Sarmiento, A. Rundquist, A. Majumdar, J. Vučković, *Optical Materials Express* **2017**, *7*, 231; K. N. Sediq, D. Coles, P. W. Fry, D. G. Lidzey, *Nanotechnology* **2016**, *27*, 225203; S. Lin, W. Zhu, Y. Jin, K. B. Crozier, *Nano Letters* **2013**, *13*, 559; C. Liu, Z. Wang, E. Li, Z. Liang, S. Chakravarty, X. Xu, A. X. Wang, R. T. Chen, D. Fan, *ACS Sensors* **2017**, *2*, 346; M. Skorobogatiy, A. V. Kabashin, *Applied Physics Letters* **2006**, *89*, 143518;

T. Zhang, S. Callard, C. Jamois, C. Chevalier, D. Feng, A. Belarouci, *Nanotechnology* **2014**, *25*, 315201; Y. Zhuo, H. Hu, W. Chen, M. Lu, L. Tian, H. Yu, K. D. Long, E. Chow, W. P. King, S. Singamaneni, *Analyst* **2014**, *139*, 1007.
[89] X. Kong, Y. Xi, P. Le Duff, X. Chong, E. Li, F. Ren, G. L. Rorrer, A. X. Wang, *Biosensors and Bioelectronics* **2017**, *88*, 63; X. Kong, Y. Xi, P. LeDuff, E. Li, Y. Liu, L.-J. Cheng, G. L. Rorrer, H. Tan, A. X. Wang, *Nanoscale* **2016**, *8*, 17285.
[90] F. Benz, M. K. Schmidt, A. Dreismann, R. Chikkaraddy, Y. Zhang, A. Demetriadou, C. Carnegie, H. Ohadi, B. de Nijs, R. Esteban, J. Aizpurua, J. J. Baumberg, *Science* **2016**, *354*, 726.
[91] R. Zhang, Y. Zhang, Z. C. Dong, S. Jiang, C. Zhang, L. G. Chen, L. Zhang, Y. Liao, J. Aizpurua, Y. Luo, J. L. Yang, J. G. Hou, *Nature* **2013**, *498*, 82.
[92] K. Kneipp, Y. Wang, H. Kneipp, L. T. Perelman, I. Itzkan, R. Dasari, M. S. Feld, *Physical Review Letters* **1997**, *78*, 1667; S. Nie, S. R. Emory, *Science* **1997**, *275*, 1102.
[93] E. C. Le Ru, M. Meyer, P. G. Etchegoin, *J Phys Chem B* **2006**, *110*, 1944; P. G. Etchegoin, M. Meyer, E. Blackie, E. C. Le Ru, *Anal Chem* **2007**, *79*, 8411; E. Blackie, E. C. Le Ru, M. Meyer, M. Timmer, B. Burkett, P. Northcote, P. G. Etchegoin, *Phys Chem Chem Phys* **2008**, *10*, 4147; E. J. Blackie, E. C. Le Ru, P. G. Etchegoin, *J Am Chem Soc* **2009**, *131*, 14466; P. P. Patra, G. V. Kumar, *J Phys Chem Lett* **2013**, *4*, 1167; P. P. Patra, R. Chikkaraddy, R. P. Tripathi, A. Dasgupta, G. V. Kumar, *Nat Commun* **2014**, *5*, 4357; D. O. Sigle, S. Kasera, L. O. Herrmann, A. Palma, B. de Nijs, F. Benz, S. Mahajan, J. J. Baumberg, O. A. Scherman, *J Phys Chem Lett* **2016**, *7*, 704.
[94] A. Ahmed, R. Gordon, *Nano Lett* **2012**, *12*, 2625.
[95] J. A. Dieringer, R. B. Lettan, 2nd, K. A. Scheidt, R. P. Van Duyne, *J Am Chem Soc* **2007**, *129*, 16249; S. L. Kleinman, E. Ringe, N. Valley, K. L. Wustholz, E. Phillips, K. A. Scheidt, G. C. Schatz, R. P. Van Duyne, *J Am Chem Soc* **2011**, *133*, 4115; M. D. Sonntag, J. M. Klingsporn, L. K. Garibay, J. M. Roberts, J. A. Dieringer, T. Seideman, K. A. Scheidt, L. Jensen, G. C. Schatz, R. P. Van Duyne, *The Journal of Physical Chemistry C* **2011**, *116*, 478; A. B. Zrimsek, A. I. Henry, R. P. Van Duyne, *Journal of Physical Chemistry Letters* **2013**, *4*, 3206; A. B. Zrimsek, N. L. Wong, R. P. Van Duyne, *Journal of Physical Chemistry C* **2016**, *120*, 5133.
[96] D. Wang, W. Zhu, M. D. Best, J. P. Camden, K. B. Crozier, *Nano Lett* **2013**, *13*, 2194.
[97] E. C. Le Ru, P. G. Etchegoin, *Annu Rev Phys Chem* **2012**, *63*, 65.
[98] H. Y. Wu, C. J. Choi, B. T. Cunningham, *Small* **2012**, *8*, 2878; H.-Y. Wu, L. Liu, M. Lu, B. T. Cunningham, *Advanced Optical Materials* **2016**, *4*, 708.
[99] P. Roelli, C. Galland, N. Piro, T. J. Kippenberg, *Nat Nanotechnol* **2016**, *11*, 164.
[100] M. K. Schmidt, R. Esteban, A. Gonzalez-Tudela, G. Giedke, J. Aizpurua, *ACS Nano* **2016**, *10*, 6291.
[101] S. Jiang, Y. Zhang, R. Zhang, C. Hu, M. Liao, Y. Luo, J. Yang, Z. Dong, J. G. Hou, *Nat Nanotechnol* **2015**, *10*, 865; Y. Zhang, Y. Luo, Y. Zhang, Y. J. Yu, Y. M. Kuang, L. Zhang, Q. S. Meng, Y. Luo, J. L. Yang, Z. C. Dong, J. G. Hou, *Nature* **2016**, *531*, 623.
[102] Y. Zhang, Y. R. Zhen, O. Neumann, J. K. Day, P. Nordlander, N. J. Halas, *Nat Commun* **2014**, *5*, 4424.
[103] A. Ahmed, R. Gordon, *Nano Lett* **2011**, *11*, 1800; W. Zhu, D. Wang, K. B. Crozier, *Nano Lett* **2012**, *12*, 6235; D. Wang, W. Zhu, Y. Chu, K. B. Crozier, *Adv Mater* **2012**, *24*, 4376.
[104] C. Steuwe, C. F. Kaminski, J. J. Baumberg, S. Mahajan, *Nano Lett* **2011**, *11*, 5339.
[105] S. Yampolsky, D. A. Fishman, S. Dey, E. Hulkko, M. Banik, E. O. Potma, V. A. Apkarian, *Nature Photonics* **2014**, *8*, 650.
[106] R. R. Frontiera, A. I. Henry, N. L. Gruenke, R. P. Van Duyne, *J Phys Chem Lett* **2011**, *2*, 1199.
[107] P. L. Stiles, J. A. Dieringer, N. C. Shah, R. P. Van Duyne, *Annu Rev Anal Chem (Palo Alto Calif)* **2008**, *1*, 601.
[108] N. Felidj, J. Aubard, G. Levi, J. R. Krenn, A. Hohenau, G. Schider, A. Leitner, F. R. Aussenegg, *Applied Physics Letters* **2003**, *82*, 3095; E. C. Le Ru, J. Grand, N. Félidj, J. Aubard, G. Lévi, A. Hohenau, J. R. Krenn, E. Blackie, P. G. Etchegoin, *The Journal of Physical Chemistry C* **2008**, *112*, 8117.
[109] J. Carolan, C. Harrold, C. Sparrow, E. Martin-Lopez, N. J. Russell, J. W. Silverstone, P. J. Shadbolt, N. Matsuda, M. Oguma, M. Itoh, G. D. Marshall, M. G. Thompson, J. C. Matthews, T. Hashimoto, J. L. O'Brien, A. Laing, *Science* **2015**, *349*, 711; H. J. Kimble, *Nature* **2008**, *453*, 1023.
[110] C. L. Degen, F. Reinhard, P. Cappellaro, *Reviews of Modern Physics* **2017**, *89*, 035002

[111] J. Haas, M. Schwartz, U. Rengstl, M. Jetter, P. Michler, B. Mizaikoff, *Analyst* **2018**, *143*, 593.
[112] F. Marquier, C. Sauvan, J.-J. Greffet, *ACS Photonics* **2017**, *4*, 2091; M. Zwierz, C. A. Pérez-Delgado, P. Kok, *Physical Review A* **2012**, *85*, 042112
[113] C. M. Caves, *Physical Review D* **1981**, *23*, 1693.
[114] J. P. Dowling, *Contemporary Physics* **2008**, *49*, 125.
[115] I. Afek, O. Ambar, Y. Silberberg, *Science* **2010**, *328*, 879.
[116] U. Rengstl, M. Schwartz, T. Herzog, F. Hargart, M. Paul, S. L. Portalupi, M. Jetter, P. Michler, *Applied Physics Letters* **2015**, *107*, 021101
[117] K. Santhosh, O. Bitton, L. Chuntonov, G. Haran, *Nat Commun* **2016**, *7*, ncomms11823.
[118] A. Crespi, M. Lobino, J. C. F. Matthews, A. Politi, C. R. Neal, R. Ramponi, R. Osellame, J. L. O'Brien, *Applied Physics Letters* **2012**, *100*, 233704.
[119] M. Gould, E. R. Schmidgall, S. Dadgostar, F. Hatami, K.-M. C. Fu, *Physical Review Applied* **2016**, *6*, 011001
[120] P. Lombardi, A. P. Ovvyan, S. Pazzagli, G. Mazzamuto, G. Kewes, O. Neitzke, N. Gruhler, O. Benson, W. H. P. Pernice, F. S. Cataliotti, C. Toninelli, *ACS Photonics* **2017**, *5*, 126.
[121] J. T. Barreiro, N. K. Langford, N. A. Peters, P. G. Kwiat, *Phys Rev Lett* **2005**, *95*, 260501.
[122] M. D. Eisaman, J. Fan, A. Migdall, S. V. Polyakov, *Rev Sci Instrum* **2011**, *82*, 071101.
[123] Y. Zhang, T. H. Wang, *Theranostics* **2012**, *2*, 631.
[124] W. R. Algar, A. J. Tavares, U. J. Krull, *Anal Chim Acta* **2010**, *673*, 1.
[125] J. T. Hugall, A. Singh, N. F. van Hulst, *ACS Photonics* **2018**, *5*, 43; G. Khitrova, H. M. Gibbs, M. Kira, S. W. Koch, A. Scherer, *Nature Physics* **2006**, *2*, 81.
[126] C. Lee, F. Dieleman, J. Lee, C. Rockstuhl, S. A. Maier, M. Tame, *ACS Photonics* **2016**, *3*, 992.
[127] F. Najafi, J. Mower, N. C. Harris, F. Bellei, A. Dane, C. Lee, X. Hu, P. Kharel, F. Marsili, S. Assefa, K. K. Berggren, D. Englund, *Nat Commun* **2015**, *6*, 5873; X. Guo, C.-l. Zou, C. Schuck, H. Jung, R. Cheng, H. X. Tang, *Light: Science & Applications* **2016**, *6*, e16249
[128] E. Bernardi, R. Nelz, S. Sonusen, E. Neu, *Crystals* **2017**, *7*, 124.
[129] D. D. B. Rao, S. Yang, J. Wrachtrup, *Physical Review B* **2015**, *92*, 081301(R).
[130] R. Schnabel, *Physics Reports* **2017**, *684*, 1.
[131] M. A. Taylor, J. Janousek, V. Daria, J. Knittel, B. Hage, H.-A. Bachor, W. P. Bowen, *Physical Review X* **2014**, *4*, 011017
[132] M. A. Taylor, J. Janousek, V. Daria, J. Knittel, B. Hage, H.-A. Bachor, W. P. Bowen, *Nature Photonics* **2013**, *7*, 229.
[133] N. P. Mauranyapin, L. S. Madsen, M. A. Taylor, M. Waleed, W. P. Bowen, *Nature Photonics* **2017**, *11*, 477.
[134] Editorial, *Nature Photonics* **2012**, *6*, 707.
[135] Editorial, *Nature Nanotechnology* **2016**, *11*, 1.
[136] M. C. Estevez, M. Alvarez, L. M. Lechuga, *Laser & Photonics Reviews* **2012**, *6*, 463.
[137] S. Rosenblum, Y. Lovsky, L. Arazi, F. Vollmer, B. Dayan, *Nat Commun* **2015**, *6*, 6788.
[138] D. A. Giljohann, D. S. Seferos, W. L. Daniel, M. D. Massich, P. C. Patel, C. A. Mirkin, *Angew Chem Int Ed Engl* **2010**, *49*, 3280.
[139] S. S. Acimovic, M. A. Ortega, V. Sanz, J. Berthelot, J. L. Garcia-Cordero, J. Renger, S. J. Maerkl, M. P. Kreuzer, R. Quidant, *Nano Lett* **2014**, *14*, 2636.
[140] X. Ni, M. Castanares, A. Mukherjee, S. E. Lupold, *Curr Med Chem* **2011**, *18*, 4206.